Contrib Mineral Petrol (2016) 171:97
DOI 10.1007/s00410-016-1307-z

ORIGINAL PAPER

Contribution of long-term hydrothermal experiments for understanding the smectite-to-chlorite conversion in geological environments

Régine Mosser-Ruck[1] · Isabella Pignatelli[2] · Franck Bourdelle[3] · Mustapha Abdelmoula[4] · Odile Barres[1] · Damien Guillaume[5] · Delphine Charpentier[6] · Davy Rousset[7] · Michel Cathelineau[1] · Nicolas Michau[8]

Received: 1 April 2016 / Accepted: 5 October 2016 / Published online: 15 October 2016
© Springer-Verlag Berlin Heidelberg 2016

Abstract The smectite-to-chlorite conversion is investigated through long-duration experiments (up to 9 years) conducted at 300 °C. The starting products were the Wyoming bentonite MX80 (79 % smectite), metallic iron and magnetite in contact with a Na–Ca chloride solution. The predominant minerals in the run products were an iron-rich chlorite (chamosite like) and interstratified clays interpreted to be chlorite/smectite and/or corrensite/smectite, accompanied by euhedral crystals of quartz, albite and zeolite. The formation of pure corrensite was not observed in the long-duration experiments. The conversion of smectite into chlorite over time appears to take place in several steps and through several successive mechanisms: a solid-state transformation, significant dissolution of the smectite and direct precipitation from the solution, which is oversaturated with respect to chlorite, allowing the formation of a chamosite-like mineral. The reaction mechanisms are confirmed by X-ray patterns and data obtained on the experimental solutions (pH, contents of Si, Mg, Na and Ca). Because of the availability of some nutrients in the solution, total dissolution of the starting smectite does not lead to 100 % crystallization of chlorite but to a mixture of two dominant clays: chamosite and interstratified chlorite/smectite and/or corrensite/smectite poor in smectite. The role of Fe/(Fe + Mg) in the experimental medium is highlighted by chemical data obtained on newly formed clay particles alongside previously published data. The newly formed iron-rich chlorite has the same composition as that predicted by the geothermometer for diagenetic to low-grade metamorphic conditions, and the quartz + Fe-chlorite + albite experimental assemblage in the 9-year experiment is close to that fixed by water–rock equilibrium.

Keywords Chlorite · Corrensite · Hydrothermal experiment · Iron–clay interaction · Hydrothermal metamorphism · Diagenetic system

Communicated by Othmar Müntener.

✉ Régine Mosser-Ruck
regine.mosser@univ-lorraine.fr

[1] Faculté des sciences et technologies, GeoRessources UMR-CNRS 7359, Université de Lorraine, Campus Aiguillettes, BP 70239, 54506 Vandœuvre-lès-Nancy, France

[2] CRPG Université de Lorraine, CNRS/INSU UMR 7358, 15 rue Notre Dame des Pauvres, 54500 Vandœuvre-lès-Nancy, France

[3] Laboratoire Génie Civil et géo-Environnement (LGCgE), Université Lille 1, Cité Scientifique, SN5, 59655 Villeneuve-d'Ascq cedex, France

[4] Laboratoire de Chimie Physique et Microbiologie pour l'Environnement (LCPME) UMR-CNRS 7564, Université de Lorraine, 405, rue de Vandoeuvre, 54601 Villers-lès-Nancy, France

[5] LMV, UMR 6524, Faculté des Sciences et Techniques, 23 rue du Dr Paul Michelon, 42023 Saint Etienne Cedex 02, France

[6] Chrono-Environnement UMR-CNRS 6249, Université de Franche-Comté, 16, Route de Gray, 25030 Besançon Cedex, France

[7] Institut National de Recherche et de Sécurité (I.N.R.S), Avenue de Bourgogne, 54500 Vandœuvre-lès-Nancy, France

[8] Agence nationale pour la gestion des déchets radioactifs (ANDRA), Parc de la Croix Blanche, 1/7 rue Jean Monnet, 92298 Châtenay-Malabry Cedex, France

Introduction and state of the art

Understanding the conditions and mechanisms of the smectite-to-chlorite transformation is of great interest in many geological environments as well as for studying the behavior of a bentonitic barrier under the thermal and chemical effects of nuclear waste storage (radioactive decay of fission products and interactions between the corrosion products of steel containers and bentonite). Occurrences of chlorite, random interstratified smectite–chlorite and ordered mixed-layered clays such as corrensite, have been described in numerous environments: hydrothermal altered volcanic rocks (Krismannsdottir 1979; Alt et al. 1986; Bettison and Schiffman 1988; Shau et al. 1990; Inoue and Utada 1991; Schiffman and Fridleifsson 1991; Bevins et al. 1991; Shau and Peacor 1992; Robinson et al. 1993; Schiffman and Staudigel 1995; Bettison-Varga and Mackinnon 1997); diagenetic systems (Hoffman and Hower 1979; Chang et al. 1986); geothermal fields (Inoue 1987; Liou et al. 1985; Robinson and Santana de Zamora 1999; Robinson et al. 2002); hydrothermal metamorphism in the oceanic crust (Alt et al. 1986; Buatier et al. 1995; Abad et al. 2003); and geological formations considered as natural analogues of a bentonite barrier in a deep geological repository for high-level radioactive waste (Pelayo et al. 2011). The conversion process has long been the subject of active debate. Several authors have reported that the reaction pathway for the conversion involves a disequilibrium smectite–chlorite mixed-layering continuous sequence with random and ordered interstratification types (Krismannsdottir 1979, 1983; Liou et al. 1985; Bettison and Schiffman 1988; Bevins et al. 1991; Schiffman and Fridleifsson 1991; Robinson et al. 1993). Others have suggested that the conversion consists of an equilibrated discontinuous sequence with corrensite, and mixed-layered smectite–corrensite and corrensite–chlorite all occurring as intermediate clays before chlorite formation (Inoue et al. 1984; Inoue 1987; Shau et al. 1990; Inoue and Utada 1991; Shau and Peacor 1992; Schiffman and Staudigel 1995; Schmidt and Robinson 1997; Beaufort et al. 1997; Murakami et al. 1999; Pelayo et al. 2011). In the second model, corrensite, which is a regular interstratified mineral (Bailey 1982; Brigatti and Poppi 1984), is considered a discrete phase in the thermodynamic sense, with a discrete stability field (Beaufort et al. 1997). Robinson et al. (2002) proposed a third mechanism consisting of a possible direct smectite-to-chlorite transition. This last model was validated by the presence of clay mineral assemblages composed of either smectite or chlorite end-members with less than 15 % mixed layers, in the altered volcanic sequence of the Chipilapa geothermal system in El Salvador (Robinson and Santana de Zamora 1999). According to the authors, the continuous or discontinuous pathways of the smectite-to-chlorite conversion are supported by X-ray diffraction, electron microprobe and TEM data. For example, HR-TEM evidence for well-developed continuous sequences of smectite–chlorite has been reported in Schiffman and Fridleifsson (1991), Robinson et al. (1993) and Bettison-Varga and Mackinnon (1997). In contrast, Inoue et al. (1984), Shau et al. (1990), Shau and Peacor (1992), Jiang and Peacor (1994a, b), Beaufort et al. (1997), Bettison-Varga and Mackinnon (1997) and Murakami et al. (1999) have shown that smectite-to-chlorite conversion series progresses in a stepwise manner from smectite to corrensite and from corrensite to chlorite via smectite–corrensite and corrensite–chlorite interstratified minerals, corrensite being considering as a single phase. Regardless of the discontinuous or continuous nature of the reaction pathway, the mechanism of the smectite-to-chlorite conversion is considered either to be the result of solid-state transformation (Bettison-Varga and Mackinnon 1997; Schmidt and Robinson 1997) or to proceed through a dissolution–crystallization process (Shau et al. 1990). Robinson et al. (2002) also suggested that the crystallographic and chemical properties of interstratified smectite/chlorite minerals are kinetically controlled by specific factors such as temperature, thermal gradient, whole-rock chemistry, grain size, and fluid/rock ratio and that the rates of dissolution/nucleation/growth can control the reaction process of the smectite-to-chlorite transition. Therefore, knowledge of the influence of certain factors on the smectite-to-chlorite conversion can provide valuable information regarding the history of the weathering processes (Kameda et al. 2011; Pelayo et al. 2011; Sone et al. 2012; Portner et al. 2015). Temperature and fluid/rock ratio are considered to be the main factors that control the smectite-to-chlorite transformation. Krismannsdottir (1979), Keith and Bargar (1988), Schiffman and Fridleifsson (1991) and Robinson and Santana de Zamora (1999) all reported that the upper limit of smectite stability is at 180–210 °C and that the initiation of the smectite-to-chlorite conversion occurs between 150 and 200 °C. According to these authors, the formation of the first chlorite layers correlates with an increase in temperature from 210 to 270 °C. Chlorite is always a minor phase at temperatures below 120 °C, but it can become the main phase at 160 °C (e.g., Curtis et al. 1985; Robinson and Santana de Zamora 1999). So, in summary, while it is assumed that the smectite transformation is initiated from 150 °C, it is difficult to relate the reaction pathways (continuous or discontinuous) or appearance of interstratified chlorite/smectite, corrensite and chlorite, to a precise range of temperatures. The porosity, the permeability of the rocks and consequently the fluid/rock ratio are also considered as important kinetic factors that affect the smectite-to-chlorite conversion (Shau et al. 1990; Shau and Peacor 1992; Schiffman and Staudigel 1995; Schmidt and Robinson 1997). Discontinuous transformation would be favored

by a high fluid/rock ratio, while continuous transformation, characterized by the presence of randomly interlayered chlorite/smectite, is interpreted as a metastable progression with incomplete recrystallization during low fluid/rock alteration (Shau and Peacor 1992; Schiffman 1995; Schiffman and Staudigel 1995). Finally, because of the wide range of compositions of interstratified smectite–chlorite minerals and corrensites reported in the literature, and in particular their variable iron and magnesium contents (Brigatti and Poppi 1984; Chang et al. 1986; Inoue and Utada 1991; Meunier et al. 1991; Pelayo et al. 2011), it is likely that these two chemical elements also play an important role in the transformation of smectite into chlorite.

In order to confirm and accurately quantify both the effects of different factors (temperature, fluid/rock ratio, iron availability) and the mechanisms of the smectite-to-chlorite conversion, experimental approaches could provide an interesting alternative. However, experiments reporting the formation of chlorite under low pressure and low temperature conditions are rare. The first hydrothermal experiments were carried out by Roberson et al. (1999), who studied the transformation of saponite to chlorite at 500, 350 °C and 2 kbar in a Fe-free system. Saponite transformed to corrensite within 6 h at 500 °C and within 22 days at 350 °C. No evidence for intermediate randomly interstratified chlorite/smectite was found as a precursor of corrensite. In an iron-poor experimental system, Mosser-Ruck et al. (2003) also demonstrated that the Mg-vermiculite from Santa Olalla (Spain) converts into complex mixed-layered clays composed of saponite, chlorite (±Mg-vermiculite) at 300 °C and 86 bar. The specific role of iron was investigated at distinct temperatures (90, 150, 250 and 300 °C) in the pioneering experimental synthesis of Guillaume et al. (2003, 2004), Wilson et al. (2006) and Lantenois et al. (2005), in the context of studies of the stability of bentonite clay barriers in nuclear waste storage. These studies were followed by investigations into the role of pH on this system (Charpentier et al. 2006; Perronnet et al. 2008; Osacký et al. 2010, Mosser-Ruck et al. 2010), and thermal gradients (Jodin-Caumon et al. 2010). And as part of the study of oxygen isotope fractionations between chlorite and water, hydrothermal granite-fluid experiments at temperature between 170 and 300 °C also demonstrated that chlorite formed from biotite (Cole and Ripley 1999). Most experimental studies concluded to the systematic dissolution of the starting clay and its replacement by Fe–phyllosilicates, mostly Fe–serpentines, appearing as small amounts of poorly crystallized grains at temperatures lower than 100 °C. Cronstedtite was also identified by Lanson et al. (2012) at 80 °C and in the absence of O_2. Iron-rich di- and trioctahedral smectites have been observed above 100 °C, and chlorites have been observed at 300 °C (Guillaume et al. 2003, 2004; Wilson et al. 2006; Charpentier et al. 2006; Mosser-Ruck et al. 2010), contradicting earlier studies that asserted that the formation of chlorite was impossible below 400 °C (Velde 1973; Small et al. 1992). The rate of the reactions mostly depends on redox conditions, pCO2, and iron/clay and liquid/solid ratios (see reviews in Mosser-Ruck et al. 2010 and Lanson et al. 2012). Thus, Mosser-Ruck et al. (2010) reported a significant rate of conversion of smectite into Fe–phyllosilicates for high water/rock (>5) and iron/clay (>0.5) ratios. Moreover, Lantenois et al. (2005) and Lanson et al. (2012) demonstrated that the reactivity of smectites was also a function of their initial iron content. At temperatures equal to or higher than 150 °C, the final mineral assemblage observed experimentally by Guillaume et al. (2003, 2004) and Mosser-Ruck et al. (2010) was composed of saponite, trioctahedral chlorite ± randomly interstratified chlorite/smectite, quartz, feldspar and zeolite.

In the work of Guillaume et al. (2003), the experimental conditions were characterized by a high temperature (300 °C), a high fluid/rock ratio (10) and a high Fe/(Fe + Mg) ratio (Fe^0 powder/bentonite mass ratio of 0.1 and Fe^0/magnetite = 1 ± an iron plate). After 9 months, they observed a partial dissolution of the di-octahedral smectite of the starting bentonite in favor of newly formed clays, identified by HR-TEM to be chlorite and saponite. The transformation of the smectite into chlorite was incomplete in this 9-month experiment; however, the mechanisms of the transformation, which remain poorly understood, were not described in the paper. The authors assumed that the scarcity of the mixed-layered chlorite/smectite minerals in their experimental system was due to the high temperature of their experiments (300 °C) which would have prevented the formation of the mixed-layered clays.

The main objective of the present paper is to answer a number of questions, including (1) what are the transformation pathways of smectite under the experimental conditions of Guillaume et al. (2003)? and (2) what is the role of iron in the smectite-to-chlorite conversion at 300 °C? In order to answer these questions, two longer duration experiments, of 25 months and 9 years, were carried out at 300 °C and under the same conditions as those of Guillaume et al. (2003). The most evolved run products are characterized in detail by a multi-technique analysis (XRD, TEM, SEM, FTIR, STXM–XANES and Mössbauer spectroscopy) and are then compared to the run products obtained in the previous study of Guillaume et al. (2003) in order to assess the conversion rate and to try to determine whether a kinetic law can be established. Modeling of the chlorite composition at the experimental temperature (Inoue et al. 2009; Bourdelle et al. 2013a) is then used to compare the nature and compositions of the experimental and predicted chlorites.

Materials and methods

The starting product belongs to a smectite group mineral. It is the MX80 Na, Ca-bentonite (Wyoming, USA), which is mostly composed of montmorillonite (79 %) and has the following structural formula determined by Guillaume et al. (2001a, b):

$$Na_{0.18}Ca_{0.10}\left(Al_{1.55}Mg_{0.28}Fe^{3+}_{0.09}Fe^{2+}_{0.08}\right)(Si_{3.98}Al_{0.02})O_{10}(OH)_2.$$

The MX80 Na, Ca-bentonite also contains detrital quartz (3 %), K-feldspar (2 %), plagioclase (9 %), carbonates (2 %), mica (3 %) and other minerals (pyrite, phosphates and hematite, 2 %), all presenting alteration traces (Guillaume 2002).

The bentonite powder (1.5 g) was mixed with metallic iron and magnetite powders in a 0.1 weight ratio, and an iron plate ($8 \times 4 \times 1$ mm^3) was also added. The solid mixture with a chlorine solution composed of NaCl (0.0207 Molal) and $CaCl_2$ (0.0038 Molal) was placed under argon atmosphere in gold-lined warm-sealed autoclaves (liquid/solid weight ratio of 10).

Experimental conditions: autoclaves were heated in a furnace at 300 °C for durations of 25 months and 9 years. The internal pressure of 86 bars is the liquid–vapor equilibrium pressure at 300 °C. At the end of experiments, the autoclaves were quenched at 25 °C and opened in a glove box under argon atmosphere.

Run solutions: run samples were immediately centrifuged in order to extract the solution. In a glove box, the pH was measured and solution aliquots were filtered through 0.025-µm filters. One aliquot of the solution was diluted ten times in HNO_3 (0.5 N) to prevent the precipitation of iron and aluminum compounds and used to measure the concentrations of major cations (Al, Ca, Fe, K, Mg, Na, Si) by induced coupled plasma optical emission spectroscopy (ICP-OES) at the LIEC laboratory (Université de Lorraine, France). A second aliquot of the solution was diluted three times in H_2O in order to determine the concentrations of SO_4^{2-} and Cl^- by ionic chromatography (IC) at the LCPME laboratory (Université de Lorraine, France).

Characterization of run product: Powder XRD patterns were recorded on a D8 Bruker diffractometer with a non-monochromatic CoKα radiation (35 kV, 45 mA). Three oriented samples were prepared: (1) air-dried samples, (2) saturated with EG and (3) heated at 550 °C for 4 h. They were analyzed by XRD over a 3°–75°2θ (maximum) range with a step size of 0.02°2θ and 3 s per step. SEM images of primary and newly formed minerals and semiquantitative chemical analyses were obtained using a cold FEG Hitachi S-4800 SEM microscope. TEM investigations were carried out at 200 kV using a Philips CM20 microscope equipped with a Si–Li detector. Chemical compositions were determined using energy-dispersive X-Ray spectroscopy (EDX). EDX spectra were recorded by means of a PGT spectrometer equipped with an ultrathin window X-Ray detector. The k_{AB} factors were determined using standards. TEM specimens were prepared by dispersing the <2-µm fraction powders in ethanol under ultrasound and evaporating a drop suspension on a carbon network like holey support film placed on a 200 mesh copper grid.

The FTIR spectrum was obtained in the mid-IR region by micro-Fourier transform infrared spectroscopy using a Bruker IFS 55 spectrometer. Measurements were taken in reflection mode. Transmission Mössbauer spectroscopy data were obtained from appropriate quantities (10 mg of Fe per cm^2) of solid samples. These were prepared under N_2 atmosphere in a glove box and then quickly transferred under inert He atmosphere to a cold-head cryostat manufactured by Advanced Research Systems, equipped with vibration isolation stand and developed in the LCPME Laboratory. Mössbauer spectra were collected in transmission mode with a constant acceleration spectrometer and a 512 multichannel analyzer. The 50-mCi source of ^{57}Co in Rh matrix was maintained at room temperature and mounted at end of a Mössbauer velocity transducer. Data were calibrated with a 25-µm-thick α-iron foil at room temperature. Measurements were taken at 8 K and with a velocity range of ±11 mm/s or an expanded velocity range of ±4 mm/s. Use of the wider range enables the possible detection of magnetically split patterns from Fe oxides, whereas the smaller range gives an optimum resolution for the sample. Analysis of the Mössbauer spectra consisted of least-square fitting the data to a combination of two-peak quadrupole components and, when present, six-peak magnetic hyperfine components. A Lorentzian-shape lines model from Recoil software (Ottawa University) was used for the peaks in both the quadrupole and magnetic components. The hyperfine parameters are CS and Δ. In Mössbauer spectroscopy, the first hyperfine interaction called the electric monopole interaction is the perturbing effect of electrons that find themselves inside the nuclear volume. It is characterized by a shift of the complete spectrum relative to the reference (calibration) material. This shift is known as the *isomer shift* (*IS*). In addition, the spectrum is shifted by a temperature- and sample-dependent quantity, the *second-order Doppler shift* (*SOD*), resulting in a net shift relative to a calibration material known the *center shift* (*CS*) which measure the resonance position and CS = IS + SOD. The second hyperfine interaction called electric field gradient (EFG) interaction occurs when (1) the nucleus has a quadrupole moment and (2) the electronic density produces an electric field gradient at the nucleus. This causes a splitting of the excited ($I = 3/2$) nuclear state into the $m = \pm 3/2$ and $m = \pm 1/2$ branches, resulting in two distinct lines. The $I = 1/2$ ground state has no quadrupole moment. The

splitting between the two sublevels (branches) is called the quadrupole splitting, *i.e., Δ*.

For simplicity, CS and Δ are measured in "mm/s" which is conventional "energy" unit in Mössbauer spectroscopy. X-ray absorption near-edge structure spectroscopy analyses (XANES) were acquired on the PolLux beamline at the Swiss Light Source (Paul Scherrer Institute—SLS, Villigen, Switzerland). The SLS synchrotron storage ring is operated at 2.4 GeV and 400 mA current in a top-up mode during data collection. The characteristics of the beamline are detailed in Raabe et al. (2008). XANES spectroscopy is carried out with a scanning transmission X-ray microscope (STXM), which allows spectra to be collected on different particles from a single stack; the variation in the $Fe^{3+}/\Sigma Fe$ ratio through the run product can be thus qualitatively evaluated. Stacks were obtained over the 690–730 eV energy range (Fe $L_{2,3}$ edge) using energy increments of 0.667 eV between 690 and 700 eV, 0.20 eV in the 700–715 eV energy range, 0.40 eV in the 715–727 eV energy range and 0.89 eV in the 727–730 eV energy range. The dwell time per pixel and energy point was 2 ms. XANES spectra were derived from areas of interest using the aXis2000 software (Hitchcock 2012). The procedure for the spectrum treatment and $Fe^{3+}/\Sigma Fe$ ratio determination is detailed in Bourdelle et al. (2013b).

Results

Mineralogical composition of the run samples

Among the non-clay phases, quartz and Na–Ca feldspars were found to be the most abundant minerals. K-feldspar and micas, observed in the starting sample, progressively disappeared over the duration of the experiment as shown by XRD results (Fig. 4a). Neither iron powder nor magnetite that had been added to the medium at the beginning of the two longest experiments (25 months and 9 years) was detected in the bulk of the run products by XRD, SEM or TEM, suggesting that these two iron sources were entirely dissolved between 9 months (see the previous study of Guillaume et al. 2003) and 25 months. However, careful examination of the iron plate from the 25-month experiment, embedded in resin and cut perpendicular to its surface, revealed corrosion pits filled with iron oxides which formed a passivation layer up to ~90 μm around the plates (Fig. 1a). These iron oxides were sometimes mixed with iron-rich silicates and pyrite (Fig. 1b). The asymmetrical corrosion of the iron plate shown in Fig. 1a is likely due to the location of the iron plate in the starting iron–clay mixture at the beginning of the experiment. One side of the iron plate was set up against the gold liner at the bottom of the vessel, and the opposite side was in contact with the experimental mixture. The surface of the iron plate in the 9-year experiment was also observed by SEM (Fig. 1c, d). It appears to be covered by several complex corrosion layers composed of a mixture of different minerals difficult to identify. A few cubic crystals of pyrite could sometimes be observed, but no pure iron oxides were found. Among the newly formed minerals observed on the iron plate of the 9-year run sample, euhedral quartz crystals of small size (500 nm to 3 μm) and large Na-rich plagioclases (1–30 μm) are abundant (Fig. 2a, d), and acicular crystals closely associated with clay particles are also often observed (Fig. 2e, d). According to SEM and TEM analysis, the composition of these elongated prisms is close to zeolite (Na-mordenite type). However, the minerals were not detected by XRD, most likely because they represent less than 5 %.

Various morphologies characterize the newly formed clays collected in the bulk of the 25-month and 9-year run samples (Fig. 3). In the 25-month run product, we observe spherical aggregates (Fig. 3a) composed of crystal "flakes" (Fig. 3b). It is not possible to discriminate between the smectite and chlorite morphologies. In the 9-year run sample, chlorite crystals are present either as aggregates of sub-parallel stacked crystals (Fig. 3c, d) or as honeycomb structures (Fig. 3e), easily identified in the TEM images (Fig. 3f).

Figure 4 presents the data obtained by X-ray diffraction on the run products from the two longest experiments (25 months and 9 years) compared with the data obtained in the shorter experiments conducted by Guillaume et al. (2003). A significant transformation of montmorillonite MX80 over time is demonstrated. The starting montmorillonite is sodic–calcic, with a wide 001 reflection centered at ~12 Å or 8.5 2*θ* (sodic pole more abundant). Between 1 and 3 months into the experiment, the reaction product appears to have still been mostly composed of swelling clays, as indicated by the AD and EG X-ray patterns (Fig. 4a, b). These clays collapsed to ~10 Å (10.2 2*θ*), due to the loss of interlayer water, after heating of the oriented preparations at 550 °C (Fig. 4c). In the 1-month experiment, the observed shift of the 00 l reflection to higher 2*θ* values (AD pattern in Fig. 4a) can be explained by changes in the interlayer composition of the smectite (Na–Ca–H exchanges). In the 3-month experiment, the shoulder toward 14 Å (7.3 2*θ*) in the AD and EG patterns of the run product can probably be interpreted as the presence, in small quantity, of a mineral belonging to the chlorite group. However, after heating at 550 °C, the clay layers collapsed at 10 Å (Fig. 4c).

Notable changes occurred between 3 and 9 months of heating. In the AD patterns of the run samples from the 9-month, 25-month and 9-year experiments, additional reflections can be observed at ~14 Å (7.3 2*θ*), ~7 Å (14.6

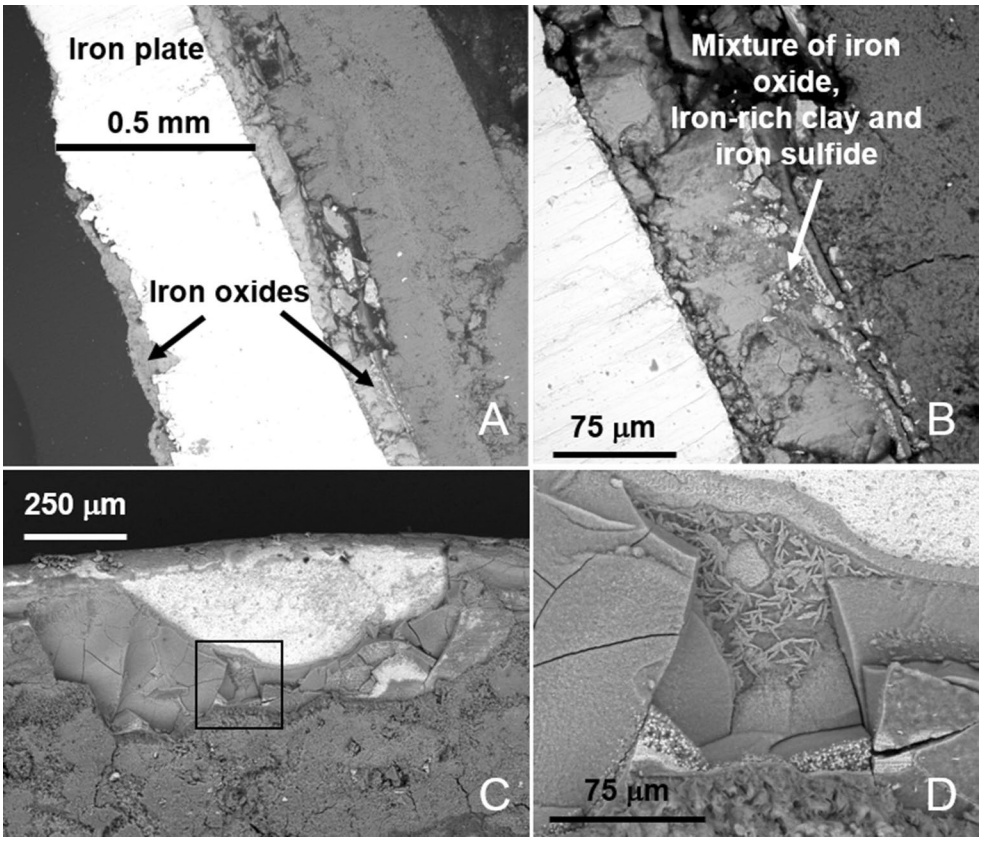

Fig. 1 SEM images of the iron plates in the 25-month (**a**, **b**) and 9-year experiments (**c**, **d**). *Black rectangle* on (**c**) refers to image (**d**). Complex corrosion layers, composed of a mixture of different minerals difficult to identify, cover the iron plate

2θ), ~4.7 Å (21.9 2θ) and ~3.54 Å (29.3 2θ), clearly indicating the presence of chlorite-like minerals or interstratified minerals containing chlorite layers (Fig. 4a). Several types of clays coexist in these samples:

1. Inherited smectites (S).
2. Mixed-layered clays, still rich in smectite, that can be interpreted as interstratified smectite/chlorite (S/C) and/or smectite/corrensite (S/Co) composed of more than 70 % smectite layers, as the EG patterns consistently show a broad reflection at ~17 Å (6.0 2θ). Most of these minerals collapsed after heating of the oriented preparations at 550 °C and were still present in the run product of the 9-month experiment.
3. Interstratified corrensite/chlorite (Co/C) and/or chlorite/smectite (C/S) containing small proportions of expandable layers (less than 10 % smectite). These minerals are characterized by broad reflections at ~14 Å (7.3 2θ) and ~7 Å (14.6 2θ) on the EG patterns of solvated preparations and preparations heated at 550 °C. These clays are abundant in the 25-month and 9-year experiments.
4. Chlorite (C). This chlorite is rich in iron, as indicated by the intensities of the 001 and 002 reflections on the AD-X-Ray patterns of the run samples and by the variation in these intensities during treatment of the oriented preparations at 550 °C (a decrease in the intensity of the 002 reflection). The presence of chlorite in the 9-month experiment was previously demonstrated by Guillaume et al. (2003) in their HR-TEM observations of run products saturated with heptylammonium.

No sharp or broad superstructure reflections around 29 Å (3.5 2θ) and 31 Å (3.3 2θ), characteristic of corrensite (Beaufort et al. 1997) can be identified in the X-ray patterns (Fig. 4b). However, since no experiments of 3- to 9-months duration were conducted, it is impossible to totally exclude the possibility that corrensite may have existed individually before the formation of chlorite and/or interstratified C/S and Co/C. The FTIR spectrum obtained for the clays removed from the iron plate in the 9-year experiment shows two bands at 3566 and 3439 cm^{-1}, typical of hydroxyl in a "brucite type" environment, supporting that these clays are chlorites (Fig. 5). The presence of

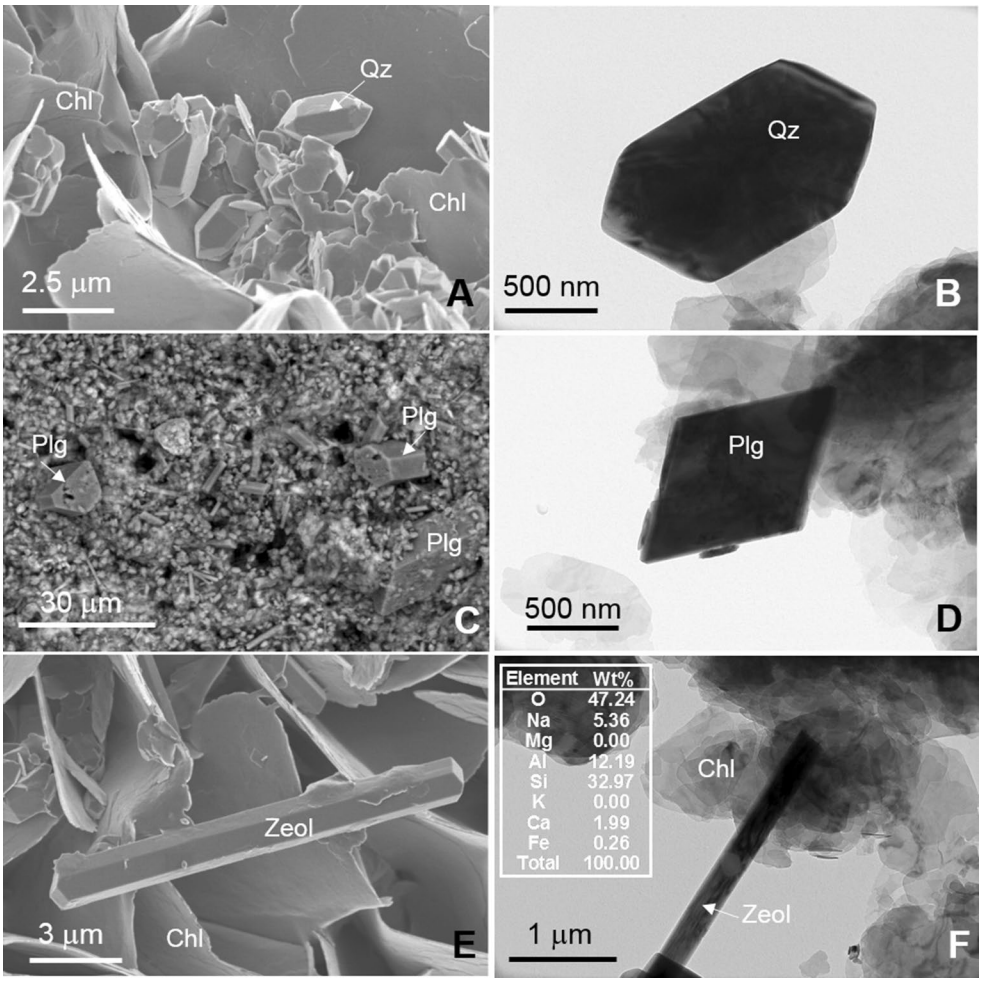

Fig. 2 SEM and TEM images of minerals collected on the surface of the iron plate of the 9-year run sample: **a**, **b** euhedral quartz (Qz) and chlorite (Chl); **c**, **d** euhedral Na-rich plagioclase (plg); **e**, **f** acicular crystal of zeolite (Zeol)

the band at 803 cm^{-1}, assigned to H–O–Fe vibrations by Hayashi and Oinuma (1965) and Farmer (1974), also indicates that newly formed clays are Fe^{2+}-trioctahedral chlorites. The other bands in the spectrum between 3800–3100 and 1800–1500 cm^{-1} can be assigned to OH and H_2O stretching vibrations and H_2O-bending vibrations, respectively, and the bands at ~1000–1200 cm^{-1} can be attributed to Si–O–Si stretching and bending vibrations typical of all silicates (Farmer 1974). The band at 654 cm^{-1} could be due to either Si–O–Fe bending bonds (Bishop et al. 2008) or OH-bending vibration (Farmer 1974).

Clay mineral chemistry

The Mössbauer spectrum of the 9-year run sample, recorded in the ±11 mm/s velocity range, reveals only paramagnetic components with asymmetrical lines assigned to chlorite and confirms the absence of metallic iron or maghemite (Fig. 6a). The second spectrum, recorded in a relatively narrow velocity range of ±4 mm/s, provides a high spectral resolution (Fig. 6b). According to structural investigations, the sample contains no known impurities and all features of the spectrum can thus be assigned to iron present in the chlorite structure. A small Fe^{3+} contribution (CS = 0.43 mm/s; Δ = 0.95 mm/s) is observed and is estimated to represent around 5 % (±1 %) of the total iron. This is associated with two Fe^{2+} contributions which have similar center shift (CS = 1.23 and 1.22 mm/s) but different values of quadrupole splitting (Δ = 2.94 and 2.59 mm/s, Table 1). These two Fe^{2+} components represent 95 % (±1 %) of the total iron content and correspond to Fe^{2+} in the M1, M2 and M3 sites of chlorites (Goodman 1979; de Grave et al. 1987; Rancourt 1994; Lougear et al. 2007). These proportions are similar to that determined by Guillaume et al. (2003) (i.e., a $Fe^{3+}/\Sigma Fe$ ratio of 0.05 for the 9-month run sample) using the same technique. In order to determine whether the $Fe^{3+}/\Sigma Fe$ of 0.05 is a mean value for the bulk clay fraction or is instead constant and characteristic of

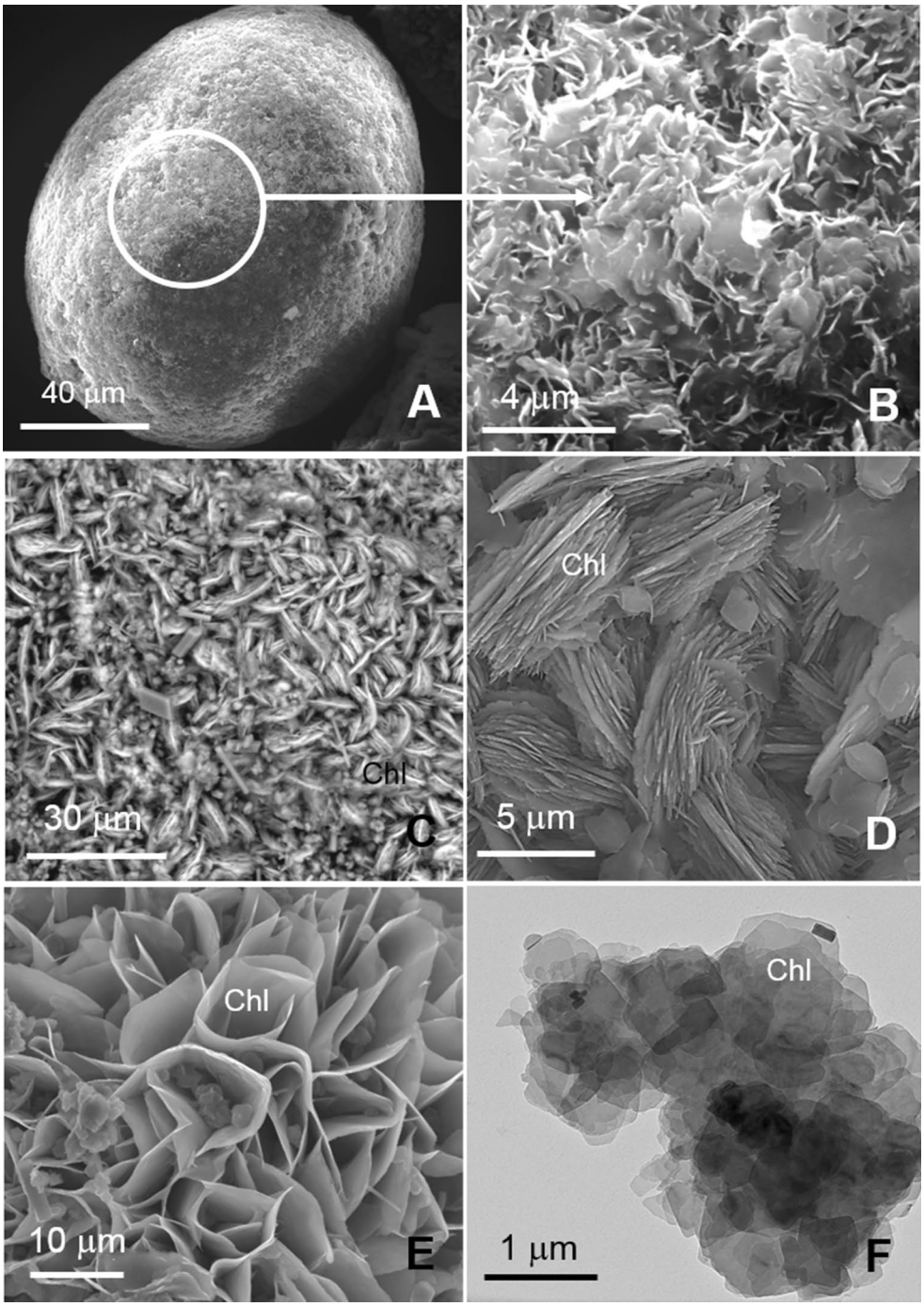

Fig. 3 SEM and TEM images of clay particles collected in the bulk of the 25-month (**a**, **b**) and the 9-year run samples (**c**–**f**). Spherical aggregates (**a**) contain crystal "flakes" (**b**) probably composed of smectite, chlorite and mixed-layer clays. In the 9-year run sample, chlorite crystals (Chl) are present either as aggregates of sub-parallel stacked crystals (**c**, **d**) or as honeycomb structures (**e**) and easily identified by their polygonal morphology in the TEM images (**f**)

the experimental medium, XANES spectra were acquired on several clay particles from the 9-year run product. The results show a strong dominance of Fe^{2+} (Fig. 7). At the L_3 edge, the intensity of the L_3-b peak, representing Fe^{3+}, is much lower than that of the L_3-a peak, which has a Fe^{2+} contribution. At the L_2 edge, the Fe^{3+} contribution is also minor compared to that of Fe^{2+}. The $Fe^{3+}/\Sigma Fe$ ratio of the run product can be determined from the spectra using the equations of Bourdelle et al. (2013b). The $Fe^{3+}/\Sigma Fe$ ratio ranges from 6 to 12 % (±3 %), depending on the particles

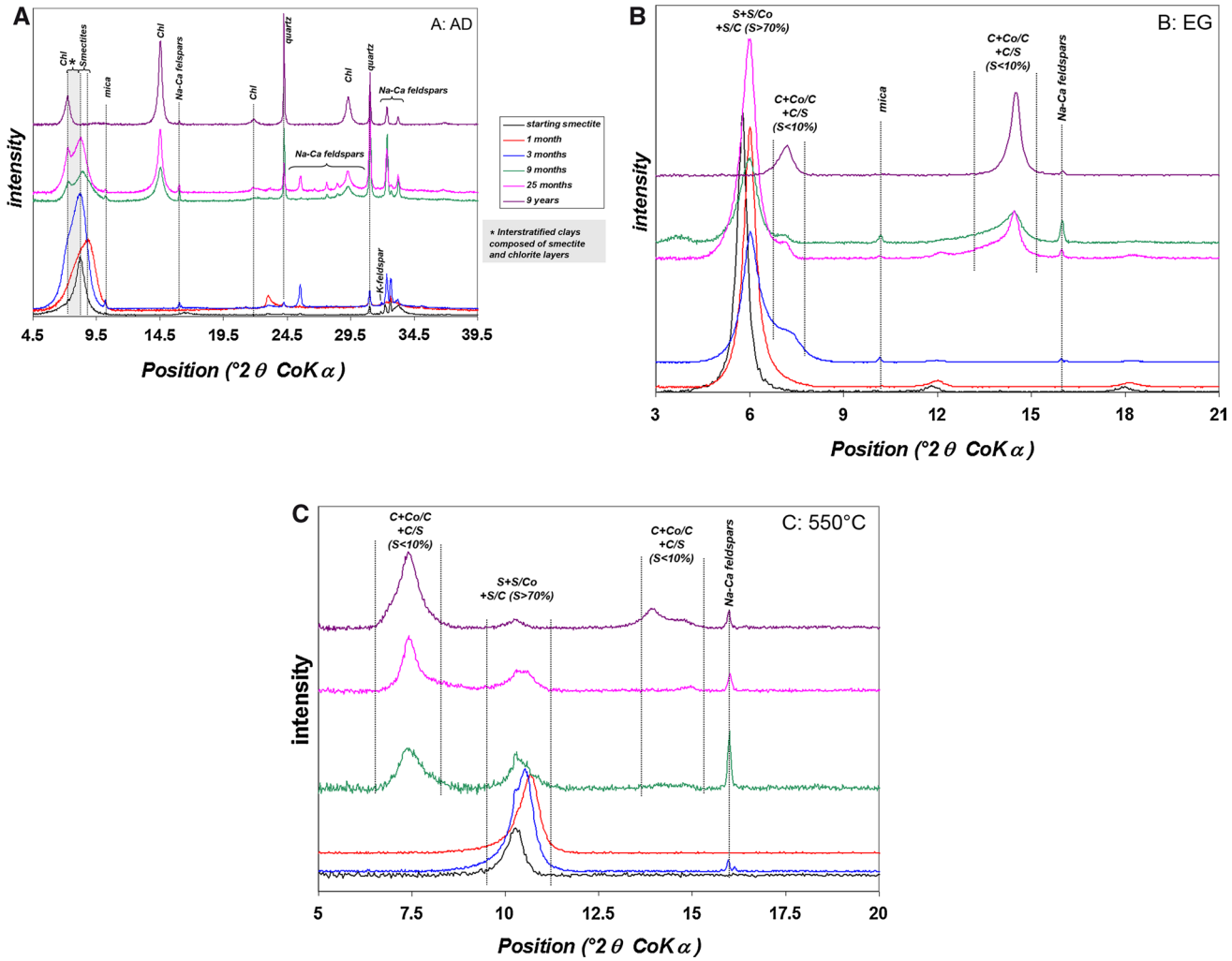

Fig. 4 XRD patterns of the starting smectite and of the run samples of the different experiments from 1 month to 9 years. **a** Air-dried, **b** ethylene glycol solvated, **c** 550 °C (*Chl* or *C* chlorite, *S* smectite, *S/C* mixed-layer smectite/chlorite rich in smectite layers, *S/Co* mixed-layer smectite/corrensite, *Co/C* mixed-layer corrensite/chlorite, *C/S* mixed-layer chlorite/smectite rich in chlorite layers)

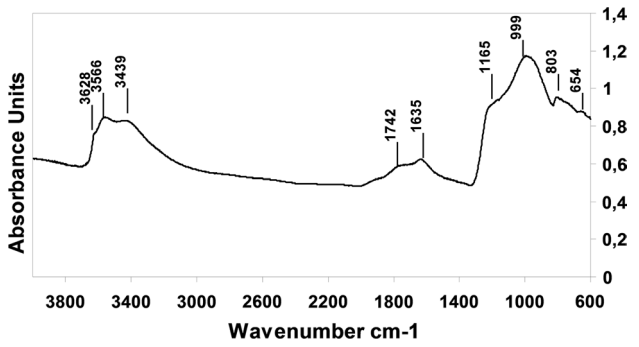

Fig. 5 IR spectra in reflexion mode of newly formed chlorites removed from the surface of the iron plate in the 9-year experiment

analyzed. This heterogeneity could be due to variations in the proportion of relict smectite present in the newly formed clay and/or (though less likely) $Fe^{3+}/\Sigma Fe$ ratio variations from one particle to another. However, qualitative evaluation of this heterogeneity shows that particles with a $Fe^{3+}/\Sigma Fe$ ratio <8 % are the most abundant, which is in agreement with the Mössbauer results.

The structural formulae for the newly formed clay minerals in the 25-month and 9-year run samples are presented in Table 2. These were calculated on the basis of 14 oxygens (10 O + 8 OH^-) from TEM–EDX analyses of isolated particles from the <2-μm fraction powders. Iron valence was fixed at 2.05 ($Fe^{3+}/\Sigma Fe_{total} = 0.05$), based on the Mössbauer data (Table 1). A wide range of compositions (in at.%) were determined for clay particles from the 25-month run, and these span the smectite and chlorite (chamosite) compositional domains (Table 2). Clay particles from the 9-year run sample have a composition close to chamosite. Very small amounts of Ca were sometimes detected by TEM–EDX in these particles. This is likely related to the presence of relict

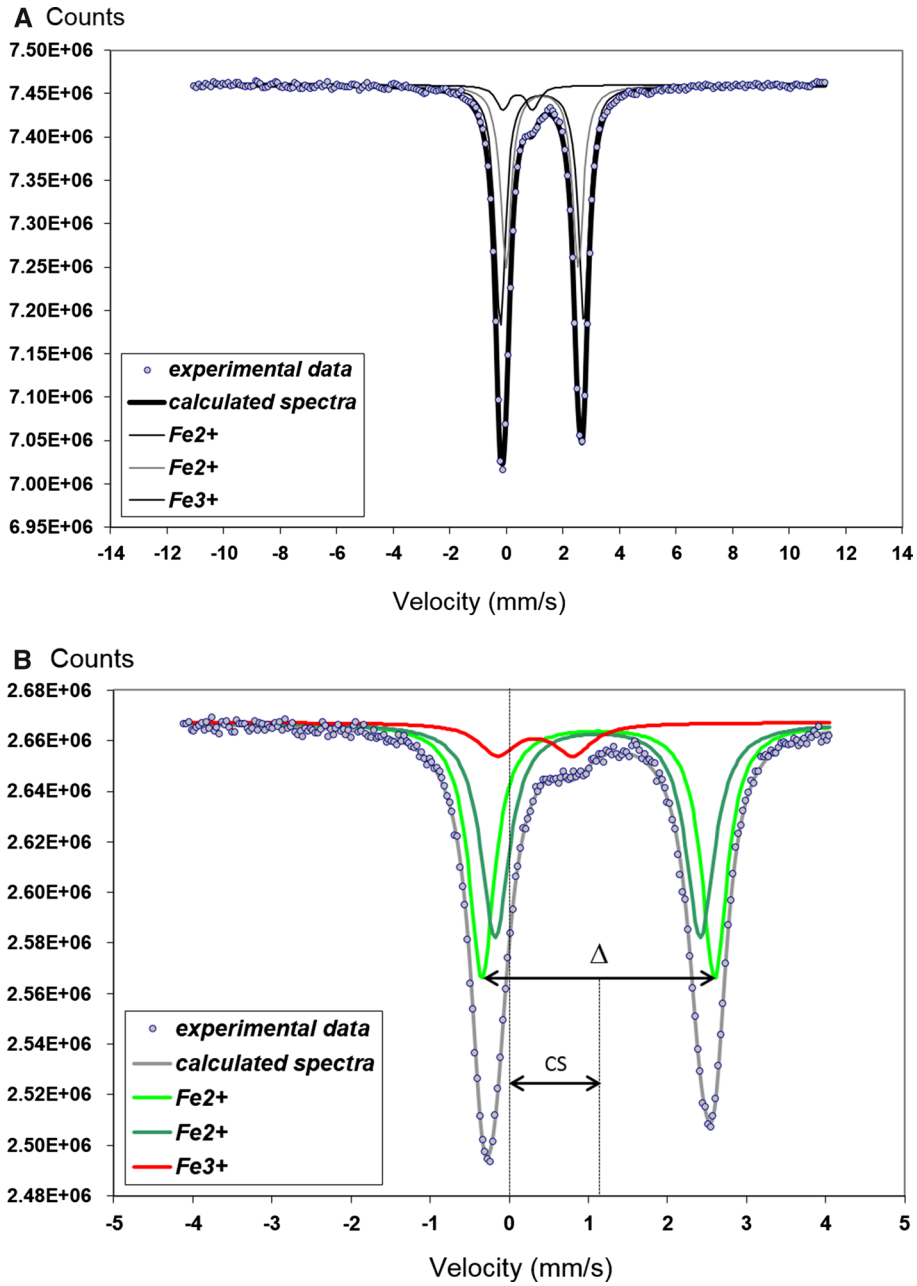

Fig. 6 **a** *Dots* 8 K Mössbauer spectrum in velocity range of ±11 mm/s. **b** *Dots* 8 K Mössbauer spectrum in velocity range of ±4 mm/s, *Green and red lines* decompositions of the spectrum. *Gray line* sum of all the contributions of the decomposition. The experimental spectra take into account the second-order Doppler shift (SOD). CS and Δ are specified on the **b** just for one site of Fe^{2+} as example of their location

Table 1 Mössbauer hyperfine parameters

Temperature: 8 K (±4 mm/s)	CS (mm/s)	Δ (mm/s)	RA (%)
Fe^{2+} chlorite	1.23	2.94	53
Fe^{2+} chlorite	1.22	2.59	42
Fe^{3+} chlorite	0.43	0.95	5

CS center shift, *Δ* quadrupole splitting, *RA* relative area (measurement accuracy is ±1 %)

layers of smectite, interstratified with chlorite layers. These relict layers are probably insufficient in proportion to produce a noticeable swelling effect on the EG-XRD patterns.

Solution chemistry

Cation and anion concentrations and pH levels for 25-month and 9-year run solutions are reported in Table 3 and are compared to those of the initial solution before and after equilibration with bentonite for 6 days at 25 °C (Guillaume et al. 2003). The measured pH values after cooling (at room temperature) are close to or slightly below than neutral pH for 25-month and 9-year experiments, respectively. Results obtained on the initial solution before and after equilibration with bentonite show that Na exchanged with Ca from the solution at 25 °C in the starting smectite. The concentrations of Si, Na, Ca and K (Mg) in the

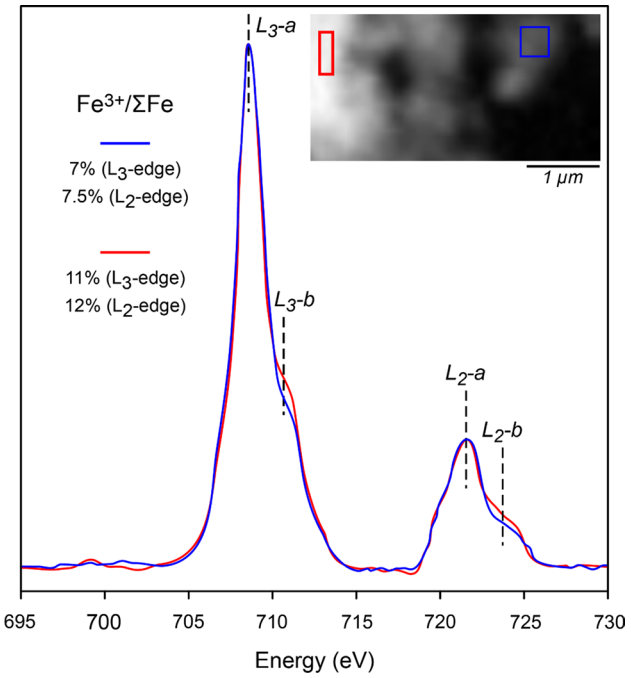

Fig. 7 Representative XANES spectra of two newly formed particles, showing $Fe^{3+}/\Sigma Fe$ ratio variability in the 9-year run sample. The spectra are normalized to the integral Fe L_3 edge intensity and are extracted from the STXM optical density image (708 eV) presented in *inset*

25-month and 9-year run solutions can be explained by equilibration of the solution with the newly formed minerals of the run products at elevated temperatures. The Si concentration is close to that fixed by the equilibrium with quartz at 300 °C (~9.6 mM). Of note, the Al, Fe and Mg contents in the experimental solutions are very low and these elements have therefore been completely reincorporated into the newly formed minerals (Al into the clays and feldspars; Fe and Mg into the chlorite and interstratified clays). The K in solution can be attributed to the dissolution of minor K-feldspar present in the starting bentonite. The presence of sulfates (S +VI) in 9-year run solution might be due to the dissolution of primary pyrites; however, evidence for this type of mineralogical alteration was neither observed in the run products nor detected by the analytical techniques used in this study.

Discussion

Mechanisms and kinetics of the smectite-to-chlorite conversion

The results of the long-duration experiments presented in this paper, alongside those obtained by Guillaume et al. (2003), confirm the absence of a single corrensite-type phase at 300 °C. Several types of clay (smectite, S/C and/or S/Co, C/S and/or Co/C, and chlorite) are shown to coexist at 300 °C for up to 9 years of heating. Figure 8 shows the X-ray patterns of oriented preparations of the starting sample and run products heated at 550 °C, and their decomposition using the DECOMPXR software of Lanson (1997). This procedure, which involves the subtraction of background and the decomposition of the superimposed peaks into elementary peaks with Gaussian and Lorentzian shapes, allows the percentages of the main clays in each run product to be calculated (Fig. 9). The different clays are interpreted to be smectite (S), interstratified S/C and/or S/Co rich in smectite layers, interstratified Co/C and/or C/S poor in smectite layers, and chlorite. The resulting percentages are shown in Fig. 9. The amount of smectite clay in the mixture decreased gradually over time. The newly formed mixed-layered clays appeared in several steps. Smectite-rich interstratified clays (S/C and/or S/Co) formed within the first 3 months of heating at 300 °C. These represented the dominant newly formed clay in the mixture. At 9 months, the amounts of chlorite (45 wt%) and Co/C and/or C/S poor in smectite layers (15 wt%) increased at the expense of the first newly formed interstratified clays. From this point onwards, chlorite was the most abundant clay in the mixture and its concentration remained stable for the remainder of the 9 years. Guillaume et al. (2003) also noted the scarcity of mixed-layered chlorite/smectite minerals in their high-resolution TEM observations of heptylammonium-saturated clay fractions (<2 μm) of the starting MX80 and 3- and 9-months run samples and suggested that the high experimental temperature (300 °C) may have prevented the formation of the mixed-layered clays. Schiffman and Fridleifsson (1991) had previously suggested that temperature is the primary control on the smectite-to-chlorite transition. In their study of the NJ-15 well in the Nesjavellir geothermal field (Iceland), discrete chlorite first appeared at 270 °C and was seen to coexist with minor amounts of R0 chlorite/smectite at higher temperatures. In the long-duration experiments presented here, the amount of interstratified C/S and/or Co/S poor in smectite increased gradually between 25 months and 9 years, reaching an abundance close to that of chlorite in the longest experiment. Under our experimental conditions, the temperature was set to 300 °C and remained constant throughout the experiments, and the liquid/clay mass ratio was initially high, equal to 10. According to some authors, these conditions should be favorable for a solid-state transformation of smectite into chlorite via corrensite, involving the growth of brucite sheets in the smectite interlayer (Bettison-Varga and Mackinnon 1997; Robinson et al. 2002). This type of reaction releases a small amount of silicon and consumes a considerable amount of water (OH^-) and might be invoked for the transformation of the smectite in the first 9 months.

Table 2 TEM–EDS analyses (in atomic %: At %) of clay particles in the 25-month and 9-year run products and recalculated structural formulae (on $O_{10}(OH)_8$ with $Fe^{3+}/\Sigma Fe_{total} = 0.05$), based on the Mössbauer data (Table 1)

Sample	TEM–EDS analyses							Structural formula (apfu)									
	Si At %	Al At %	Fe At %	Mg At %	K At %	Na At %	Ca At %	Si	Al(IV)	Al(VI)	Fe2+	Fe3+	Mg	K	Na	Ca	I.C.
25 months	16.90	10.74	7.99	1.81	0.10	1.05	0.43	3.91	0.09	2.40	1.76	0.09	0.42	0.02	0.05	0.10	0.27
	16.95	10.45	10.32	1.97	0.00	0.00	0.37	3.80	0.20	2.14	2.20	0.12	0.44	0.00	0.00	0.08	0.17
	13.88	9.53	12.80	2.52	0.01	0.00	0.37	3.35	0.65	1.64	2.93	0.15	0.61	0.00	0.00	0.09	0.18
	13.09	10.12	13.16	2.69	0.02	0.00	0.24	3.17	0.83	1.62	3.03	0.16	0.65	0.00	0.00	0.06	0.12
	13.91	9.50	13.11	2.44	0.06	0.00	0.32	3.34	0.66	1.62	2.99	0.16	0.59	0.01	0.00	0.08	0.17
	13.83	9.43	12.01	2.49	0.05	0.00	0.32	3.40	0.60	1.72	2.80	0.15	0.61	0.01	0.00	0.08	0.17
	14.09	9.79	12.62	2.40	0.03	0.00	0.41	3.36	0.64	1.70	2.86	0.15	0.57	0.01	0.00	0.10	0.20
	14.99	9.79	11.39	2.17	0.01	0.00	0.44	3.56	0.44	1.89	2.57	0.14	0.52	0.00	0.00	0.10	0.21
	15.76	10.59	15.24	2.72	0.01	0.02	0.47	3.33	0.67	1.57	3.06	0.16	0.57	0.00	0.00	0.10	0.21
	14.72	8.99	13.67	1.33	0.00	0.00	0.86	3.49	0.51	1.61	3.07	0.16	0.31	0.00	0.00	0.20	0.41
	14.52	9.67	12.63	2.61	0.00	0.00	0.35	3.42	0.58	1.70	2.83	0.15	0.61	0.00	0.00	0.08	0.16
	13.77	9.80	13.62	2.23	0.00	0.00	0.34	3.28	0.72	1.61	3.08	0.16	0.53	0.00	0.00	0.08	0.16
	17.02	10.26	8.60	1.79	0.19	0.03	0.66	3.92	0.08	2.28	1.88	0.10	0.41	0.04	0.01	0.15	0.35
	14.74	9.60	12.21	2.64	0.00	0.00	0.31	3.48	0.52	1.74	2.74	0.14	0.62	0.00	0.00	0.07	0.15
	14.81	10.56	14.71	2.46	0.00	0.00	0.36	3.27	0.73	1.61	3.09	0.16	0.54	0.00	0.00	0.08	0.16
	14.49	9.22	13.11	2.83	0.03	0.00	0.35	3.41	0.59	1.58	2.93	0.15	0.67	0.01	0.00	0.08	0.17
	15.77	10.40	9.77	1.65	0.27	0.05	0.49	3.71	0.29	2.16	2.19	0.12	0.39	0.06	0.01	0.12	0.30
	14.21	9.62	13.06	2.94	0.08	0.00	0.26	3.34	0.66	1.61	2.92	0.15	0.69	0.02	0.00	0.06	0.14
	15.22	10.23	11.27	1.57	0.14	0.02	0.31	3.59	0.41	2.01	2.53	0.13	0.37	0.03	0.00	0.07	0.18
Average	14.86	9.89	12.22	2.32	0.05	0.06	0.41	3.48	0.52	1.80	2.71	0.14	0.53	0.01	0.00	0.09	0.20
Standard deviation	1.17	0.51	1.95	0.44	0.07	0.25	0.15	0.22	0.22	0.26	0.41	0.02	0.11	0.02	0.01	0.03	0.08
9 years	9.51	9.41	12.19	3.48	0.00	0.00	0.07	2.71	1.29	1.39	3.30	0.17	0.99	0.00	0.00	0.02	0.04
	10.54	9.84	12.43	3.49	0.00	0.00	0.14	2.83	1.17	1.46	3.17	0.17	0.94	0.00	0.00	0.04	0.08
	10.72	9.91	14.21	2.51	0.00	0.00	0.13	2.80	1.20	1.40	3.53	0.19	0.66	0.00	0.00	0.03	0.07
	9.88	9.45	11.96	3.11	0.03	0.00	0.12	2.80	1.20	1.47	3.22	0.17	0.88	0.01	0.00	0.03	0.08
	10.22	9.32	12.76	3.25	0.00	0.00	0.00	***2.82***	***1.18***	***1.39***	***3.34***	***0.18***	***0.90***	***0.00***	***0.00***	***0.00***	***0.00***
	10.10	9.58	12.44	3.00	0.00	0.00	0.12	2.80	1.20	1.46	3.28	0.17	0.83	0.00	0.00	0.03	0.07
	10.23	9.22	10.51	3.23	0.03	0.00	0.13	2.96	1.04	1.62	2.89	0.15	0.93	0.01	0.00	0.04	0.08
	10.37	9.45	12.39	2.96	0.00	0.06	0.10	2.86	1.14	1.47	3.25	0.17	0.82	0.00	0.02	0.03	0.07
	10.89	9.45	12.23	3.26	0.00	0.00	0.09	2.94	1.06	1.49	3.14	0.17	0.88	0.00	0.00	0.02	0.05
	10.40	8.89	12.48	2.03	0.00	0.00	0.19	2.96	1.04	1.49	3.38	0.18	0.58	0.00	0.00	0.05	0.11
	10.89	9.98	12.93	2.95	0.00	0.00	0.07	2.88	1.12	1.51	3.24	0.17	0.78	0.00	0.00	0.02	0.04
	11.03	9.88	12.82	3.00	0.00	0.09	0.17	2.90	1.10	1.50	3.20	0.17	0.79	0.00	0.02	0.04	0.11

Table 2 continued

Sample	TEM–EDS analyses							Structural formula (apfu)									
	Si At %	Al At %	Fe At %	Mg At %	K At %	Na At %	Ca At %	Si	Al(IV)	Al(VI)	Fe2+	Fe3+	Mg	K	Na	Ca	I.C.
	10.65	9.51	11.80	2.73	0.00	0.00	0.13	2.95	1.05	1.59	3.11	0.16	0.76	0.00	0.00	0.04	0.07
	14.02	11.19	15.34	2.53	0.01	0.00	0.15	3.10	0.90	1.58	3.23	0.17	0.56	0.00	0.00	0.03	0.07
	10.33	9.04	11.86	2.45	0.00	0.01	0.12	2.95	1.05	1.54	3.22	0.17	0.70	0.00	0.00	0.03	0.07
Average	10.65	9.61	12.56	2.93	0.00	0.01	0.12	2.88	1.12	1.49	3.23	0.17	0.80	0.00	0.00	0.03	0.07
Standard deviation	1.02	0.54	1.09	0.41	0.01	0.03	0.05	0.10	0.10	0.07	0.14	0.01	0.13	0.00	0.01	0.01	0.03

apfu atoms per formula units, *IC* interlayer charge = Na + K + 2Ca

The "final" composition of chlorite is italic and bold in the table

Table 3 pH and chemistry of 25-month and 9-year run solutions

Samples	Solutions compositions (mM)									
	pH (25 °C)	Al	Ca	Fe	K	Mg	Na	Si	Cl(−I)	S(+VI)
Initial solution (Guillaume et al. 2003)	6.40	0.00	3.80	0.00	0.00	0.00	20.80	0.00	28.30	0.00
Initial solution equilibrated with bentonite 6 days at 25 °C (Guillaume et al. 2003)	7.20	0.00	0.67	0.02	0.46	0.16	55.33	0.25	30.04	nd
25 months	7.20	<DL	5.35	0.78	7.24	0.46	101.13	14.13	27.45	0.00
9 years	6.1	0.01	0.58	0.01	2.91	0.01	22.34	8.16	29.17	0.19

DL detection limit, *nd* not determined

Standard deviation of the measurements is 10 %

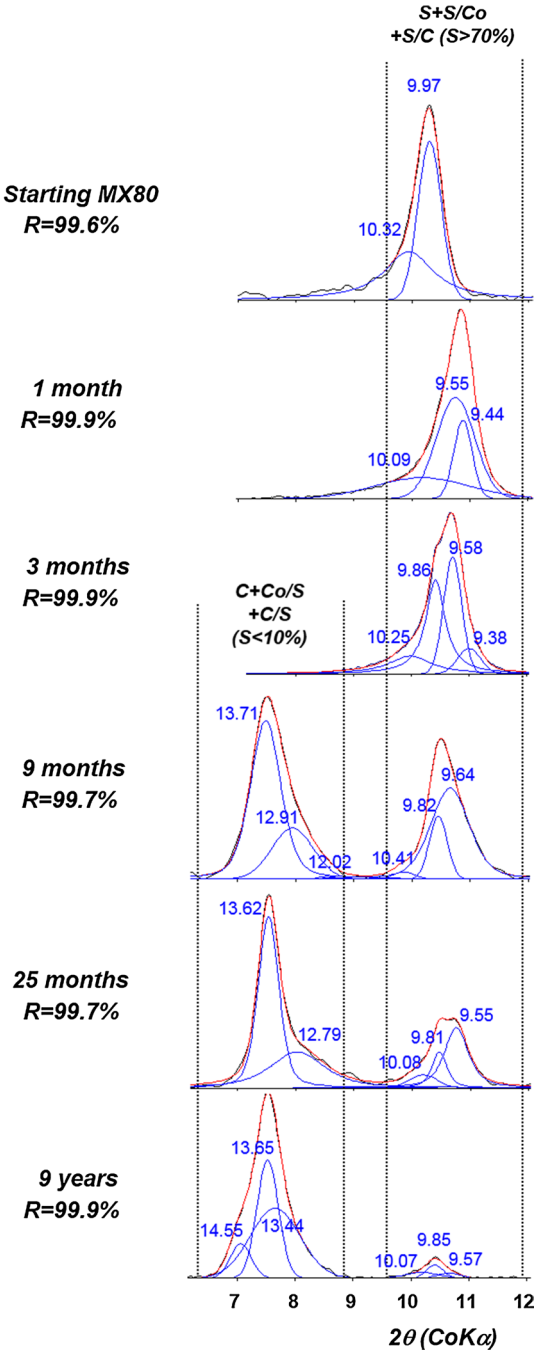

Fig. 8 Decomposition of 550 °C-XRD patterns in the 6°–12° 2θ CoKα region for the starting smectite and for run samples. *C* chlorite, *S* smectite, *S/C* mixed-layer smectite/chlorite rich in smectite layers, *S/Co* mixed-layer smectite/corrensite, *Co/C* mixed-layer corrensite/chlorite, *C/S* mixed-layer chlorite/smectite rich in chlorite layers. Values of spacing distances in Å are reported over each decomposition peak

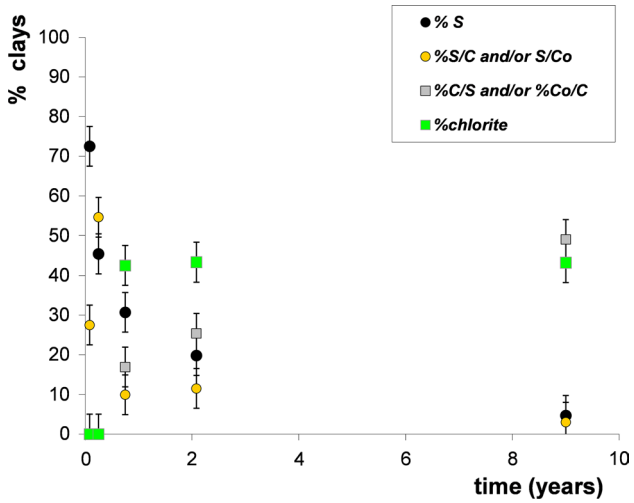

Fig. 9 Kinetic of chlorite, smectite and mixed-layer clays formation in the experimental conditions of this study (300 °C, liquid/clay ratio = 10 and iron (Fe powder + magnetite)/clay ratio = 0.1). *C* chlorite, *S* smectite, *S/C* mixed-layer smectite/chlorite rich in smectite layers, *S/Co* mixed-layer smectite/corrensite, *Co/C* mixed-layer corrensite/chlorite, *C/S* mixed-layer chlorite/smectite rich in chlorite layers

However, in order to explain the smectite–chlorite conversion via interstratified chlorite/smectite clays and the formation of discrete chlorite, a second mechanism can also be invoked. This requires the dissolution of the tetrahedral sheets in the smectite layer and the conversion of remnant octahedral sheets into a brucite layer with chemical adjustments of adjacent tetrahedral sheets in the neighboring smectite layers. This second mechanism consumes less water but releases more silicon, magnesium and/or iron (Robinson et al. 2002).

Our experiments at 300 °C demonstrate that several types of clay coexist in the same reaction products. This suggests that the transformation of smectite into chlorite involves a number of mechanisms which operate almost simultaneously (solid-state transformation, dissolution–crystallization, direct precipitation) and are accompanied by a continuous dissolution of the starting smectite. The smectite-to-chlorite conversion is also strongly dependent on the availability of nutrients (Si, Fe, Mg) and processes of dissolution/nucleation/crystallization (Srodon 1999).

Data for the experimental solutions from Guillaume et al. (2003) and from this study show that solid-state transformation is probably the dominant mechanism operating in the short-duration experiments (1–3 months), where the experimental solutions were seen to be slightly acidic and poor in Si, Fe, Mg (Guillaume et al. 2003). In contrast, in longer duration experiments (in particular over 25 months), the experimental solutions are enriched in Si, Mg, Ca and Na, indicating a higher dissolution rate of inherited smectite to form both chlorite and chlorite-rich and/or corrensite-rich interstratified clays as shown by the polygonal morphology of newly formed crystals observed by TEM (Fig. 3f). The assumption of two successive

mechanisms, and also the direct precipitation of chlorite, as has already been proposed by some authors (Meunier et al. 1991; Robinson et al. 2002), requires continuous dissolution of the starting smectite and metallic iron introduced in the experiment. The role of the fluid composition and the water/rock ratio in determining the stability of the different clays has been recognized in a number of studies (Cathelineau and Nieva 1985; Shau and Peacor 1992; Schiffman and Staudigel 1995; Robinson et al. 2002). According to these authors, individual layer silicate phases (as opposed to interlayered phases) can occur in samples in contact with high fluid fluxes. For example, Cathelineau and Nieva (1985) observed the coexistence of newly formed individual smectite and chlorite, precipitated from hydrothermal solutions at temperatures of between 250 and 300 °C in active geothermal systems. These arguments could explain the rapid formation of discrete chlorite (after 3 months) under our experimental conditions (i.e., with a liquid/clay ratio of 10). Nevertheless, our experiments at 300 °C demonstrate that despite a very long experimental duration of 9 years, interstratified clays such as Co/C and/or C/S poor in smectite layers can still coexist with Fe-rich chlorite.

Evolution of the chemical composition of clays over time and comparison with data from the literature

Figure 10 presents the evolution of the chemical composition of the newly formed clays in all experiments (1 month to 9 years) from the data published by Guillaume et al. (2003) and the new data from the present study. Also shown for comparison are the various compositions of corrensite, interstratified chlorite/smectite and corrensite/chlorite found in the literature. The black crosses in Fig. 10a–c show a theoretical continuous sequence for the interstratified chlorite/smectite minerals based on the two extreme compositions of smectite and chlorite and a progressive increase in the proportion of chlorite in steps of 10 %.

In the shorter experiments (1 and 3 months), the clays show a slight chemical evolution, involving cation exchanges in interlayer position, sometimes correlated with the decrease in Si content and a slight Fe + Mg enrichment (Fig. 10a, b). This evolution can be interpreted as a transformation of the starting montmorillonite of the MX80 bentonite into (Fe,Mg)-smectite (saponite like) and interstratified S/C and/or S/Co with more than 70 % smectite layers (Fig. 10c). The Fe/Mg of the clays in the 1- and 3-months experiments ranges between the Fe/Mg of typical smectites and chlorites (Fig. 10b) proposed by Shau et al. (1990). In tuffaceous and volcanic rich sandstones, saponite has already been recognized as a possible precursor of chlorite and chlorite/smectite minerals (Iijima and Utada 1971; Chang et al. 1986).

Newly formed clays in the 9-month experiment present two kinds of chemical evolution (green data-points on the graphs in Fig. 10). Some clays (represented by light green points) exhibit a typical corrensite composition, with an Fe/Mg ratio of around 0.93 (Shau et al. 1990) and an Fe/(Fe + Mg) ratio of around 0.5, close to the composition of clay minerals described by Meunier et al. (1991) as corrensite and/or C/S (<20 %). Other newly formed clays in this experiment (dark green points) are characterized by higher Fe/Mg ratios (>2.75) and Fe/(Fe + Mg) ratios (around 0.8) that are typical of interstratified C/S and/or Co/C rich in Fe-chlorite layers (>70 %) or possibly also in Fe–serpentine layers (Fig. 10d). The neoformation of Fe–serpentine was previously mentioned by Wilson et al. (2006) in experiments on the stability of bentonite at 250 °C in the presence of native Fe, magnetite and aqueous solution. The existence of two compositional trends for clays from a single experiment can be explained by the Fe availability in the experimental medium. At the nearest contact with the Fe plate, the high iron concentration in solution favors the crystallization of chlorite. With increasing distance from the Fe plate, the Fe/Mg ratio decreases, and the formation of corrensite would be promoted. Thus, the compositions of the newly formed clays in the sample of the 9-month experiment reflect a heterogeneous experimental system, with different rates of dissolution that most likely correspond to the different origins of iron (metal powder, iron plate and magnetite). The important role of Fe in the smectite-to-chlorite transformation was previously highlighted by Brigatti and Poppi (1984). Although Beaufort and Meunier (1994) indicated that the chemical composition of corrensite is poorly constrained because of the scarcity of pure corrensite, Brigatti and Poppi (1984) had proposed that this mineral presents a large compositional variability due to the compositional range of both the swelling component and the non-swelling component. According to these authors, from a statistical analysis of chemical data of the literature, Mg occupies 40–80 % of the octahedral sites and 15–30 % of tetrahedral sites are filled by Al. The proportion of corrensite relative to chlorite is controlled principally by the Fe/Mg ratio of the fluids or bulk rocks (Curtis et al. 1985; Shau et al. 1990; Inoue and Utada 1991; Pelayo et al. 2011). A ratio Fe/(Fe + Mg) < 0.5 in composition of this kind of clays favors the formation of corrensite, whereas at higher Fe contents, the crystallization of chlorite is promoted. The chemistry of the newly formed clays in the two long-duration experiments, characterized by Fe/Mg ratios higher than 2.75 and Fe/(Fe + Mg) > 0.8, is typical of chlorite and Co/C and/or C/S rich in chlorite (Fig. 10b, c). The crystallization of chlorite is promoted by the high iron content in solution. The magnetite and iron powders have been completely dissolved, as demonstrated by the

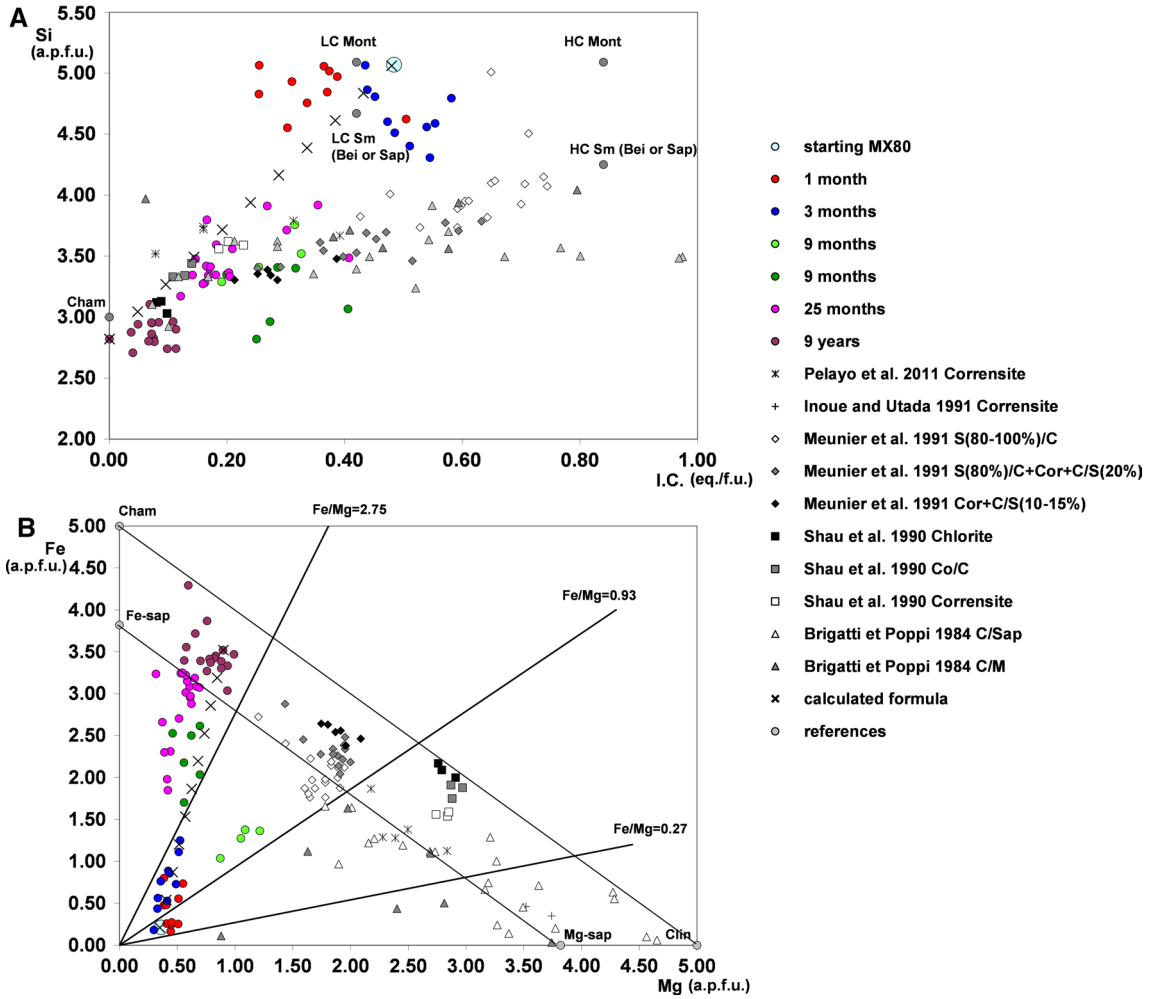

Fig. 10 Clay minerals composition of the run samples. Formulae are recalculated on 14 oxygens in diagrams. *Black crosses* in graphs **a**–**c** shows a theoretical continuous sequence for the interstratified chlorite/smectite minerals, based on the two extreme compositions of smectite and chlorite, and with a progressive increase in the chlorite proportion by steps of 10 %. **a** Si versus IC (IC = K + Na + 2Ca); **b** Fe versus Mg; the values 2.75, 0.93 and 0.27 are assigned to Fe/Mg in chlorite, corrensite and smectite, respectively, from the schematic structural models of Shau et al. (1990); **c** Fe/(Fe + Mg) versus Si; **d** Al^{VI}–Mg–Fe diagram. Other than for Fe/(Fe + Mg), the axis units are atoms per formula unit (apfu). Reference minerals are: low-charge montmorillonite: LC Mont: $(Al_{1.67}R^{2+}_{0.33})(Si_4)O_{10}(OH)_2M^{+}_{0.33}$; high-charge montmorillonite: HC Mont: $(Al_{1.33}R^{2+}_{0.67})(Si_4)O_{10}(OH)_2M^{+}_{0.67}$; low-charge beidellite: LC–Sm (Bei): $Al_2\ (Si_{3.67}Al_{0.33})O_{10}(OH)_2\ M^{+}_{0.33}$; high-charge beidellite: HC–Sm (Bei): $Al_2\ (Si_{3.33}Al_{0.67})O_{10}(OH)_2\ M^{+}_{0.67}$; low-charge Mg–saponite: LC–Sm(Mg–Sap): $[Si_{3.67}Al_{0.33}]\ Mg_3O_{10}(OH)_2\ M^{+}_{0.33}$; high-charge Mg–saponite: HC–Sm(Mg–Sap): $[Si_{3.33}Al_{0.67}]\ Mg_3O_{10}(OH)_2\ M^{+}_{0.67}$; low-charge Fe–saponite: LC–Sm(Fe–Sap): $[Si_{3.67}Al_{0.33}]\ Fe_3O_{10}(OH)_2\ M^{+}_{0.33}$; high-charge Fe–saponite: HC–Sm(Fe–Sap): $[Si_{3.33}Al_{0.67}]\ Fe_3O_{10}(OH)_2\ M^{+}_{0.67}$; chamosite: Cham: $(Fe_3{}^{2+})(Fe_2{}^{2+}Al)(Si_3Al)O_{10}(OH)_8$; clinochlore: Clin: $(Mg_3)(Mg_2Al)(Si_3Al)O_{10}(OH)_8$; Fe–serpentine (cronstedtite like): Fe–Serp: $(Fe^{2+}_{4.76}Fe^{3+}_{1.42})\ (Si_{2.24}\ Fe^{3+}_{1.62}Al_{0.14})O_{10}(OH)_8$

XRD results, and thus the iron plate is only remaining source of iron in the 25-month and 9-year experiments. Because of the crystallization of minerals on its surface, the iron plate is almost totally passivated. The availability of iron is thus slowed down, and the supply of iron may even ceased. This probably explains why a complete transformation of mixed-layer C/S and/or C/Co into chlorite is not possible and why these two types of clay coexist in equal relative abundances in the run product of the 9-year experiment.

Figure 10c also highlights the existence of gaps in our experimental sequence of smectite-to-chlorite transformation: first, between random interstratified S/C (or Co) and corrensite, and second, between corrensite and interstratified C/S (or Co) rich in chlorite. The same gaps in the transformation sequence have also been observed in geological environments, as has the coexistence of these three end-member minerals (Inoue et al. 1984). Kinetic factors may also be significant in determining the structure and the composition of the phases that form. C/S was scarce in the

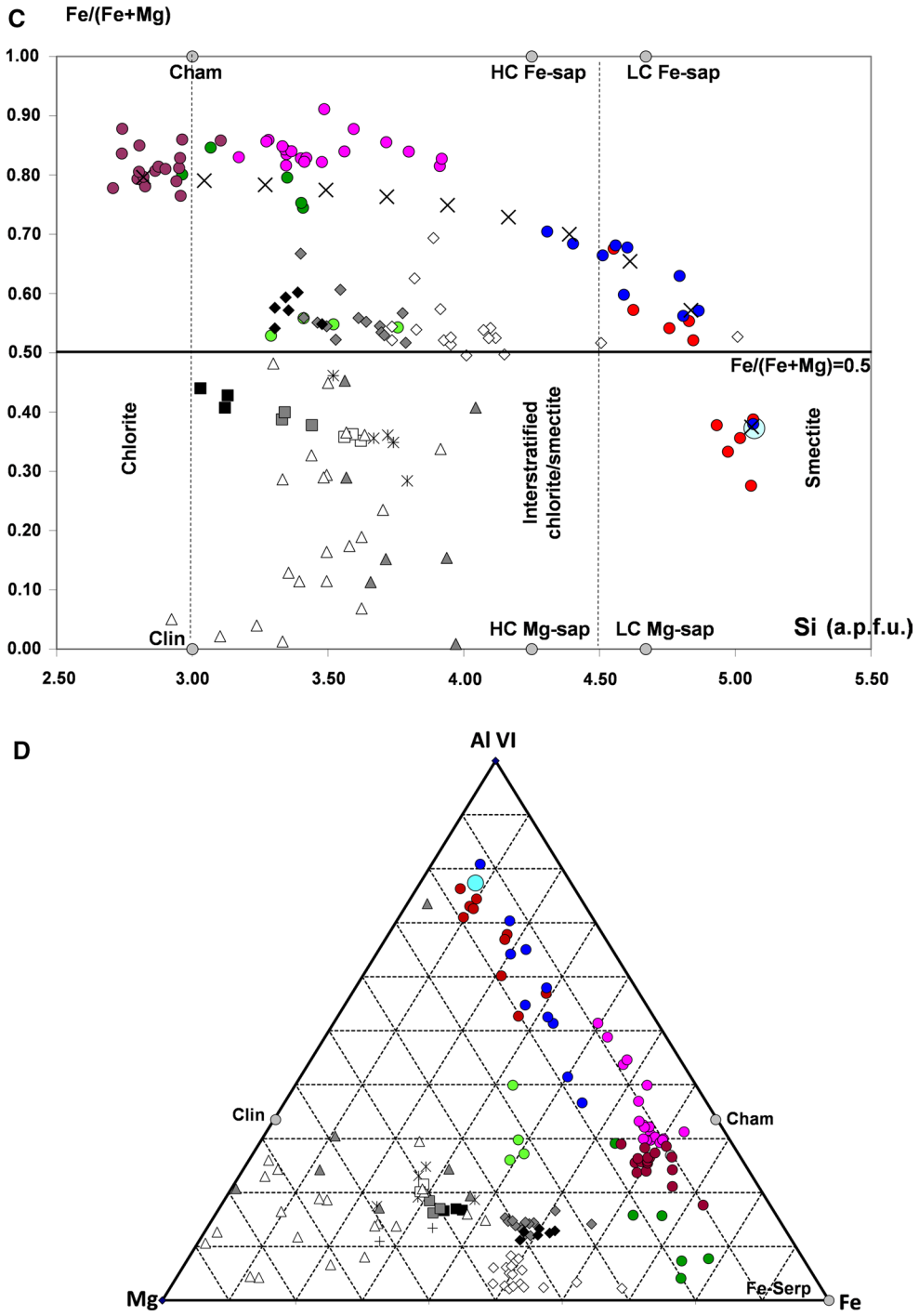

Fig. 10 continued

laboratory experiments of Guillaume et al. (2003) and Wilson et al. (2006), not only because the temperature of their experiments was too high, but also because the experiments were too short, preventing the dissolution of both the random S/C and/or S/Co rich in smectite and limiting the corrosion of iron metal for supplying Fe to the experimental system.

If the total dissolution of iron can be expressed as $Fe^0 + 2\,H_2O \rightarrow H_2 + 2\,OH^- + Fe^{2+}$, then the global reaction of the smectite-to-chlorite conversion in the 9-year experiment will be:

$$3\,\text{Smectite} + 3\,\text{Fe} + 4\,H_2O \rightarrow 1\,\text{Chlorite} + 3\,\text{Quartz} + 2\,\text{Albite} + 3\,H_2(+\text{Zeolite})$$

where $Na_{0.18}Ca_{0.10}(Al_{1.55}Mg_{0.28}Fe^{3+}_{0.09}Fe^{2+}_{0.08})(Si_{3.98}Al_{0.02})O_{10}(OH)_2$ is the formula for smectite and $(Fe^{2+}_{3.34}Fe^{3+}_{0.18}Mg_{0.90}Al_{1.39}\square_{0.19})(Si_{2.82}Al_{1.18})O_{10}(OH)_8$ is the formula for chlorite ("extreme" composition at 300 °C, see Table 2).

Thermodynamic approach

The crystallization of new phases is controlled by the availability of the constituent elements through the dissolution of the starting products, the coexistence of metastable minerals during the evolution of the system and the P–T conditions. Therefore, for the given physicochemical parameters, the composition of newly formed chlorite in the 9-year run product should be consistent with the temperature of the system (300 °C) according to thermodynamic predictions. Several thermodynamic models and semiempirical models that take into account changes in composition with temperature (geothermometers) have been proposed in the literature (e.g., Walshe 1986; Vidal et al. 2006; Inoue et al. 2009; Bourdelle et al. 2013a; Lanari et al. 2014). Here, the Inoue et al. (2009) thermometer was chosen because it is very sensitive to compositional changes (Bourdelle et al. 2013c) and because the ferric iron content is available and well constrained in the run products (the Bourdelle et al. (2013a) thermometer gives similar results, for a pure Fe^{2+} system). The results are presented in a T–Si–R^{2+} diagram (Wiewiora and Weiss 1990; Bourdelle and Cathelineau 2015) in Fig. 11, based on the estimated Fe^{3+} content. The TEM analyses of the 9-year run product show lower Si contents and higher R^{2+} contents (Fe^{2+}+Mg) than in the 25-month run product, giving rise to higher temperatures. From the unrealistic, very low temperatures for the 25-month sample, which result from the presence of remaining smectite (30 %), the data trend toward the 300 °C isoline. Therefore, most of the 9-year compositions refer to temperatures of between 250 and 300 °C, 300 °C being associated with the most extreme/pure-chlorite compositions. These results are consistent with the experimental parameters and with the crystallization of 300 °C-Fe-chlorite. Several of the points indicate lower temperatures, sometimes under 200 °C (gray points in Fig. 11). These values might be explained by the presence of a small proportion of relict smectite or a superimposition of chlorite and newly formed quartz (which was abundant), implying an overestimation of Si in the formula, and/or by the limited availability of Fe locally to complete the smectite-to-chlorite transformation.

Thus, despite the contamination by relict smectite, the most evolved compositions and the thermometric predictions are in accordance with the expected progressive crystallization of equilibrated Fe-pure-chlorite.

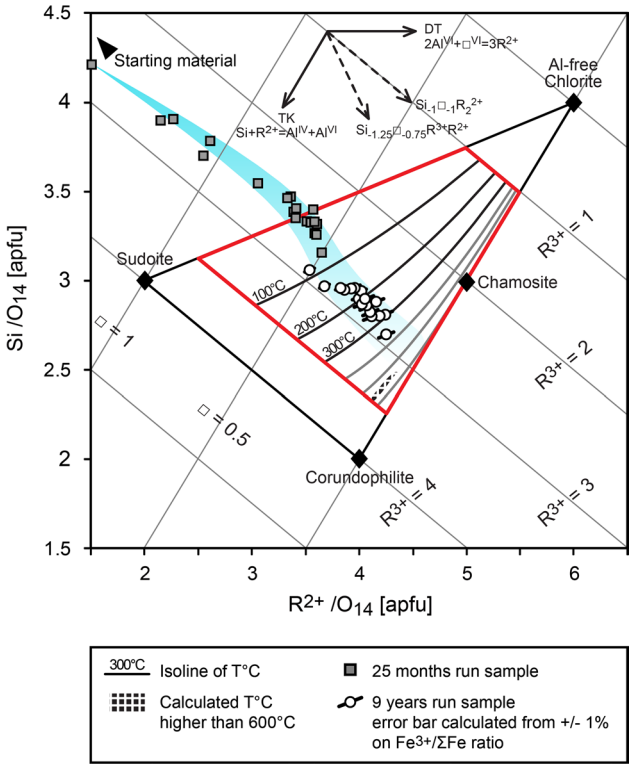

Fig. 11 Chlorite chemical compositions obtained with TEM–EDX analysis of 9-year experiment plotted in T–R^{2+}–Si diagram (Wiewiora and Weiss 1990; Bourdelle and Cathelineau 2015). R^{3+} refers to trivalent cations (Al and Fe^{3+}) and R^{2+} to divalent cations (Fe^{2+} and Mg). The isolines of temperature were calculated with the quadratic equation of Inoue et al. (2009) in the $3.5 < R^{3+} < 1.5$ apfu compositional range; Fe^{3+} content is considered. End-members used by the thermometer are identified; all analyses on a $O_{10}(OH)_8$ basis. TK and DT refer to the Tschermak ($Si + R^{2+} = {}^{IV}Al + {}^{VI}Al$) and the di-trioctahedral ($2\,{}^{VI}Al + {}^{VI}\square = 3\,R^{2+}$) exchanges, respectively

Conclusion

The transformation of smectite to chlorite via interstratified clays is usually interpreted in the literature to be a response to a progressive increase in temperature during diagenesis and low-grade metamorphism in different kinds of geological environment. However, the fluid flux (the fluid/rock ratio related to the porosity/permeability of the rocks) is also reported to be an important factor controlling the mechanism of the smectite-to-chlorite conversion. In this study, the temperature was fixed at 300 °C from the beginning of the experiment, making the difference between the experimental conditions and the natural conditions in geological environments. After 9 years at 300 °C and in the presence of iron and a high liquid/clay ratio (10), the smectite is almost entirely dissolved and two

main clay phases appear (>90 %), a Fe-rich chlorite (chamosite like) and a mixed-layer clay composed of mostly chlorite layers (>70 %) interstratified with smectite and/or corrensite. From TEM and SEM images, XRD and EDX data obtained on solids of the run samples, and chemical data obtained on experimental solutions, the two long-duration experiments of this study, carried out under the same conditions as those of Guillaume et al. (2003), allow us to clarify our understanding of the smectite-to-chlorite conversion. A discontinuous model is proposed, involving several steps of transformation and combined with two mechanisms: (1) a solid-state transformation to form the first random interstratified clays, which are rich in smectite and considered as metastable phases; followed by (2) steps of dissolution–crystallization, which increase stability toward equilibrium states and lead to the precipitation of chlorite-rich interstratified clays (C/S and or Co/C) and the separate phase chlorite. Pure corrensite was not observed in this study. If it exists, it is scarce, probably because of the high Fe/(Fe + Mg) ratio in the experimental medium which would have inhibited corrensite formation and favored the crystallization of chlorite. Direct precipitation of iron-rich chlorites from the experimental solution saturated with respect to this mineral was also envisaged in the longer duration experiments. For the first time, this experimental study demonstrates that the Fe/Mg ratio is a decisive factor in controlling the formation of pure corrensite. The thermometric model used predicts a chlorite composition at 300° C which was obtained by experiment, showing that the experimental and thermodynamic results are consistent and imply that "equilibrium" (in a system with quartz) is reached.

Acknowledgments We are grateful to the Paul Scherrer Institute, Swiss Light Source, and especially to Benjamin Watts. This research was financially supported by ANDRA – Agence Nationale pour la gestion des Dechets RadioActifs (the French National Agency for the Management of Radioactive Waste). Alice Williams is greatly thanked for proof reading the paper and her corrections of English. The authors wish also to thank O. Müntener, editor in chief, and the anonymous reviewers for comments and suggestions that greatly improved the paper.

References

Abad I, Jimenez-Millan J, Molina JM, Nieto F, Vera JA (2003) Anomalous reverse zoning of saponite and corrensite caused by contact metamorphism and hydrothermal alteration of marly rocks associated with subvolcanic bodies. Clay Clay Miner 51:543–554

Alt JC, Honnorez J, Laverne C, Emmermann R (1986) Hydrothermal alteration of a 1 km section through the upper oceanic crust, DSDP Hole 504B: mineralogy, chemistry, and evolution of seawater-basalt interactions. J Geophys Res 91:10309–10335

Bailey SW (1982) Nomenclature for regular interstratifications. Am Mineral 67:394–398

Beaufort D, Meunier A (1994) Saponite, corrensite and chlorite-saponite mixed-layers in the Sancerre-Couy deep drill-hole (France). Clay Miner 29:47–61

Beaufort D, Baronnet A, Lanson B, Meunier A (1997) Corrensite: a single phase or a mixed-layer phyllosilicate in the saponite-to-chlorite conversion series? A case of Sancerre-Couy deep drill-hole (France). Am Mineral 82:109–124

Bettison LA, Schiffman P (1988) Compositional and structural variations of phyllosilicates from the Point Sal ophiolite, California. Am Mineral 73:62–76

Bettison-Varga L, Mackinnon IDR (1997) The role of the randomly mixed-layered chlorite/smectite in the transformation of smectite to chlorite. Clay Clay Miner 45:506–516

Bevins RE, Robinson D, Rowbotham G (1991) Compositional variations in mafic phyllosilicates from regional low-grade metabasites and applications of the chlorite geothermometer. J Metamorp Geol 9:711–721

Bishop JL, Lane MD, Dyar MD, Brown J (2008) Reflectance and emission spectroscopy study of four groups of phyllosilicates: smectites, kaolinite-serpentines, chlorites and micas. Clay Miner 43:35–54

Bourdelle F, Cathelineau M (2015) Low-temperature chlorite geothermometry: a graphical representation based on a T–R^{2+}–Si diagram. Eur J Mineral 27:617–626

Bourdelle F, Parra T, Chopin C, Beyssac O (2013a) A new chlorite geothermometer for diagenetic to low-grade metamorphic conditions. Contrib Mineral Petrol 165:723–735

Bourdelle F, Benzerara K, Beyssac O, Cosmidis J, Neuville DR, Brown GE, Paineau E (2013b) Quantification of the ferric/ferrous iron ratio in silicates by scanning transmission X-ray microscopy at the Fe $L_{2,3}$-edges. Contrib Mineral Petrol 166:423–434

Bourdelle F, Parra T, Beyssac O, Chopin C, Vidal O (2013c) Clay minerals as geo-thermometer: a comparative study based on high spatial analyses of illite and chlorite in Gulf Coast sandstones (Texas, USA). Am Mineral 98:914–926

Brigatti MF, Poppi L (1984) Crystal chemistry of corrensite: a review. Clay Clay Miner 32:391–399

Buatier M, Monnin C, Früh-Green G, Karpoff AM (1995) Mechanisms of Mg phyllosilicate formation in a hydrothermal system at a sedimented ridge (Middle Valley, Juan de Fuca). Contrib Mineral Petrol 122:134–151

Cathelineau M, Nieva D (1985) A chlorite solid solution geothermometer. Contrib Mineral Petrol 91:235–244

Chang HK, Mackenzie FT, Schoonmaker I (1986) Comparisons between the diagenesis of dioctahedral and trioctahedral smectite, Brazilian offshore basins. Clay Clay Miner 31:407–423

Charpentier D, Devineau K, Mosser-Ruck R, Cathelineau M, Villieras F (2006) Bentonite-iron interactions under alkaline condition: an experimental approach. Appl Clay Sci 32:1–13

Cole RD, Ripley EM (1999) Oxygen isotope fractionation between chlorite and water from 170 to 350 °C: A preliminary assessment based on partial exchange and fluid/rock experiments. Geochim Cosmochim Acta 63:449–457

Curtis CD, Hughes CR, Whiteman JA, Whittle CK (1985) Compositional variation within some sedimentary chlorites and some comments on their origin. Mineral Mag 49:375–386

De Grave E, Vandenbruwaene J, Van Bockstael M (1987) ^{57}Fe Mössbauer spectroscopic analysis of chlorite. Phys Chem Miner 15:173–180

Farmer VC (1974) The layer silicates. In: Farmer VC (ed) The infrared spectra of minerals. Monograph 4. Mineralogical Society, London, pp 331–363

Goodman, BA, Bain DC (1979) Mössbauer spectra of chlorites and their decomposition products. In: Mortland MM, Farmer VC (eds) International clay conference 1978, pp 65–74. Elsevier, Amsterdam

Guillaume D (2002) Etude expérimentale du système fer—smectite en présence de solution à 80 °C et 300 °C. Ph.D. Thesis. Université Henri Poincaré. 3 avril 2002, p 216

Guillaume D, Neaman A, Mosser-Ruck R, Dubessy J, Cathelineau M, Villiéras F (2001a) Experimental study of hydrothermal reactivity of bentonite at 80 and 300 °C in the presence of iron and/or iron oxides. Berichte der Deutsch en Mineralogischen Gesellshaft, Beihefte zum Eur J Miner 13:69

Guillaume D, Pironon J, Ghanbaja J (2001b) Valence determination of iron in clays by electron energy loss spectroscopy. Berichte der Deutschen Mineralogischen Gesellshaft, Beihefte zum Eur J Miner 13:70

Guillaume D, Neaman A, Cathelineau M, Mosser-Ruck R, Peiffert C, Abdelmoula M, Dubessy J, Villieras F, Baronnet A, Michau N (2003) Experimental synthesis of chlorite from smectite at 300 °C in the presence of metallic Fe. Clay Miner 38:281–302

Guillaume D, Neaman A, Cathelineau M, Mosser-Ruck R, Peiffert C, Abdelmoula M, Dubessy J, Villiéras F, Michau N (2004) Experimental study of the transformation of smectite at 80 °C and 300 °C in the presence of Fe oxides. Clay Miner 39:17–34

Hayashi H, Oinuma K (1965) Relationship between infrared absorption spectra in the region of 450-900 cm^{-1} and chemical composition of chlorite. Am Mineral 50:476–483

Hitchcock AP (2012) aXis (2000) analysis of X-ray images and spectra. McMaster University, Hamilton

Hoffman J, Hower J (1979) Clay minerals assemblages as low grade metamorphic geothermometers: application to the thrust fault disturbed belt of Montana, USA. In aspects of diagenesis, SEPM special publications, vol 26, pp 55–79

Iijima A, Utada M (1971) Present-day zeolite diagenesis of the Neogene geosynclinals deposits in the Niigata oilfield, Japan. In: Gould RF (ed) Molecular sieve zeolites-I. Advance in chemistry series 101. American Chemical Society, Washington, pp 342–349

Inoue A (1987) Conversion of smectite to chlorite by hydrothermal diagenetic alterations, Hokuroku Kuroko mineralization area, northeast Japan, pp 158–164. In: Schultz LG, van Olphen H, Mumpton FA (eds) Proceedings of the international clay conference, Denver, 1985. The Clay Minerals Society, Bloomington

Inoue A, Utada M (1991) Smectite-to-chlorite transformation in thermally metamorphosed volcanoclastic rocks in the Kamikita area, North Honshu, Japan. Am Mineral 76:628–640

Inoue A, Utada M, Nagata H, Watanabe T (1984) Conversion of trioctahedral smectite to interstratified chlorite/smectite in Pliocene acidic pyroclastic sediments of the Ohyu district, Akita Prefecture, Japan. Clay Sci 6:103–106

Inoue A, Meunier A, Patrier-Mas P, Rigault C, Beaufort D, Vieillard P (2009) Application of chemical geothermometry to low-temperature trioctahedral chlorites. Clay Clay Miner 57:371–382

Jiang WT, Peacor DR (1994a) Prograde transitions of corrensite and chlorite in low-grade pelitic rocks from the Gaspé Peninsula, Quebec. Clays Clay Miner 42:497–517

Jiang WT, Peacor DR (1994b) Formation of corrensite, chlorite and chlorite-mica stacks by replacement of detrital biotite in low-grade pelitic rocks. J Metamorph Geol 12:867–884

Jodin-Caumon MC, Mosser-Ruck R, Rousset D, Randi A, Cathelineau M, Michau N (2010) Effect of a thermal gradient on iron clay interactions. Clay Clay Miner 58:667–681

Kameda J, Ujiie K, Yamaguchi A, Kimura G (2011) Smectite to chlorite conversion by frictional heating along a subduction thrust. Earth Planet Sci Lett 305:161–170

Keith TE, Bargar KE (1988) Petrology and hydrothermal mineralogy of U.S. Geological Survey Newberry 2 Drill Core From Newberry Caldera, Oregon. J Geophys Res 93:10174–10190

Krismannsdottir H (1979) Alteration of basaltic rocks by hydrothermal activity at 100–300 °C. In: Mortland MM, Farmer VC (eds) Proceedings of the 6th international clay conference, pp 359–367. Elsevier, Amsterdam

Krismannsdottir H (1983) Chemical evidence from Icelandic geothermal systems as compared to submarine geothermal systems. In: PA Roan, K Böstrom, L Laubier, KL Smith Jr (eds) Hydrothermal processes at Seafloor Spreading Centers. NATO Conference Series IV 12, Plenum, New York, pp 291–301

Lanari P, Wagner T, Vidal O (2014) A thermodynamic model for di-trioctahedral chlorite from experimental and natural data in the system MgO–FeO–Al2O3–SiO2–H2O: applications to P–T sections and geothermometry. Contrib Miner Petrol 167(2):19. doi:10.1007/s00410-014-0968-8

Lanson B (1997) Decomposition of experimental X-ray diffraction patterns (profile fitting): a convenient way to study clay minerals. Clay Clay Miner 45:132–146

Lanson B, Lantenois S, Van Aken PA, Bauer A, Plançon A (2012) Experimental investigation of smectite interaction with metal iron at 80 °C: structural characterization of newly formed Fe-rich phyllosilicates. Am Mineral 97:864–871

Lantenois S, Lanson B, Muller F, Bauer A, Jullien M, Plançon A (2005) Experimental study of smectite interaction with metal Fe at low temperature: 1. Smectite destabilization. Clay Clay Miner 53:597–612

Liou JG, Seki Y, Guillemette RN, Sakai H (1985) Composition and paragenesis of secondary minerals in the Onikobe geothermal system, Japan. Chem Geol 49:1–20

Lougear A, Grodzicki M, Bertoldi C, Trautwein AX, Steiner K, Amthauer G (2007) Mössbauer and molecular orbital study of chlorites. Phys Chem Miner 27:258–269

Meunier A, Inoue A, Beaufort D (1991) Chemiographic analysis of trioctahedral smectite-to-chlorite conversionseries from the Ohyu Caldera, Japan. Clays Clay Miner 39(4):409–415

Mosser-Ruck R, Pironon J, Guillaume D, Cathelineau M (2003) Experimental alteration of Mg-vermiculite under hydrothermal conditions: formation of mixed-layered saponite chlorite minerals. Clay Miner 38:303–314

Mosser-Ruck R, Cathelineau M, Guillaume D, Charpentier D, Rousset D, Barres O, Michau N (2010) Effects of temperature, pH, and iron/clay and liquid/clay ratios on experimental conversion of dioctahedral smectite to berthierine, chlorite, vermiculite, or saponite. Clay Clay Miner 58:280–291

Murakami T, Sato T, Inoue A (1999) HRTEM evidence for the process and mechanism of saponite-to-chlorite conversion through corrensite. Am Mineral 84:1080–1087

Osacký M, Šucha V, Czímerová A, Madejová J (2010) Reaction of smectites with iron in a nitrogen atmosphere at 75 °C. Appl Clay Sci 50:237–244

Pelayo M, Garcia-Romero E, Labajo MA, Perez del Villar L (2011) Occurrence of Fe-Mg rich smectites and corrensite in the Morron de Mateo bentonite deposit (Cabo de Gata region, Spain): a natural analogue of the bentonite barrier in a radwaste repository. Appl Geochem 26(7):1153–1166

Perronnet M, Jullien M, Villiéras F, Raynal J, Bonnin D, Bruno G (2008) Evidence of a critical content in Fe(0) on Foca7 bentonite reactivity at 80 °C. Appl Clay Sci 38:187–202

Portner RA, Clague DA, Helo C, Dreyer BM, Paduan JB (2015) Contrasting styles of deep-marine pyroclastic eruptions revealed from Axial Seamount push core records. Earth Planet Sci Lett 423:219–231

Raabe J, Tzvetkov G, Flechsig U, Böge M, Jaggi A, Sarafimov B, Vernooij MGC, Huthwelker T, Ade H, Kilcoyne D, Tyliszczak T, Fink RH, Quitmann C (2008) PolLux: a new facility for soft X-ray spectromicroscopy at the Swiss Light Source. Rev Sci Instrum 79

Rancourt DG (1994) Mössbauer spectroscopy of minerals. II. Problem of resolving *cis* and *trans* octahedral Fe^{2+} sites. Phys Chem Miner 21:250–257

Roberson HE, Reynolds RC, Jenkins DM (1999) Hydrothermal synthesis of corrensite: a study of the transformation of saponite to corrensite. Clay Clay Miner 47(2):212–218

Robinson D, Santana de Zamora A (1999) The smectite to chlorite transition in the Chipilapa geothermal system, El Salvador. Am Mineral 84:607–619

Robinson D, Bevin RE, Rowbotham G (1993) The characterization of mafic phyllosilicates in low grade metabasalts from eastern North Greenland. Am Mineral 78:377–390

Robinson D, Th Schmidt S, Santana de Zamora A (2002) Reaction pathways and reaction progress for the smectite-to-chlorite transformation: evidence from hydrothermally altered metabasites. J Metamorph Geol 20:167–174

Schiffman P (1995) Low grade metamorphism of mafic rocks. Rev Geophys 33:81–86

Schiffman P, Fridleifsson GO (1991) The smectite–chlorite transition in drillhole Nj-15, Nesjavellir geothermal field, Iceland: XRD, BSE, and electron microprobe investigations. J Metamorph Geol 9:679–696

Schiffman P, Staudigel U (1995) The smectite to chlorite transition in a fossil seamount hydrothermal system: the basement complex of La Palma, Canary Islands. J Metamorp Geol 13:487–498

Schmidt S, Robinson D (1997) Metamorphic grade and porosity/permeability controls on mafic phyllosilicate distributions in a regional zeolite to greeschist facies transition of the North shore Volcanic Group, Minnesota. Geol Soc Am Bull 109:683–697

Shau YH, Peacor DR (1992) Phyllosilicates in hydrothermally altered basalts from DSDP Hole 504B, Leg 83—a TEM and AEM study. Contrib Miner Petrol 112:119–133

Shau YH, Peacor DR, Essene EJ (1990) Corrensite and mixed-layer chlorite/corrensite in metabasalts from northern Taiwan: TEM/AEM, EMPA, XRD and optical studies. Contrib Miner Petrol 105:123–142

Small JS, Hamilton DL, Habesch S (1992) Experimental simulation of clay precipitation within reservoir sandstones 1: techniques and examples. J Sediment Petrol 62:508–519

Sone H, Shimamoto T, Moore DE (2012) Frictional properties of saponite-rich gouge from a serpentinite-bearing fault zone along the Gokasho-Arashima Tectonic Line, Central Japan. J Struct Geol 38:172–182

Srodon J (1999) Nature of mixed-layer clays and mechanisms of their formation and alteration. Annu Rev Earth Planet Sci 27:19–53

Velde B (1973) Phase equilibria studies in the system MgO–AlO–SiO–UO: chlorite and associated minerals. Mineral Mag 39:297–312

Vidal O, de Andrade V, Lewin E, Muñoz M, Parra T, Pascarelli S (2006) P–T-deformation-Fe^{3+}/Fe^{2+} mapping at the thin section scale and comparison with XANES mapping: application to a garnet-bearing metapelite from the Sambagawa metamorphic belt (Japan). J Metamorph Geol 24:669–683

Walshe JL (1986) A six-component chlorite solid solution model and the conditions of chlorite formation in hydrothermal and geothermal systems. Econ Geol 81:681–703

Wiewiora A, Weiss Z (1990) Crystallochemical classifications of phyllosilicates based on the unified system of projection of chemical composition: II. The chlorite group. Clay Miner 25:83–92

Wilson J, Cressey G, Cressey B, Cuadros J, Ragnarsdottir KV, Savage D, Shibata M (2006) The effect of iron on montmorillonite stability. (II) Experimental investigation. Geochim Cosmochim Acta 70:323–336